Mechanical studies towards a silicon micro-strip super module for the ATLAS inner detector upgrade at the high luminosity LHC

2014 JINST 9 P04018

(http://iopscience.iop.org/1748-0221/9/04/P04018)

PUBLISHED BY IOP PUBLISHING FOR SISSA MEDIALAB
RECEIVED: *December 18, 2013*
REVISED: *March 5, 2014*
ACCEPTED: *March 20, 2014*
PUBLISHED: *April 22, 2014*

Mechanical studies towards a silicon micro-strip super module for the ATLAS inner detector upgrade at the high luminosity LHC

G. Barbier,[a] F. Cadoux,[a] A. Clark,[a,*] M. Endo,[b] Y. Favre,[a] D. Ferrere,[a] S. Gonzalez-Sevilla,[a] K. Hanagaki,[b] K. Hara,[e] G. Iacobucci,[a] Y. Ikegami,[f] O. Jinnouchi,[c] D. La Marra,[a] K. Nakamura,[f] R. Nishimura,[d] E. Perrin,[a] W. Seez,[a] Y. Takubo,[f] R. Takashima,[d] S. Terada,[f] K. Todome,[c] Y. Unno[f] and M. Weber[a]

[a] *DPNC, University of Geneva, 24 rue Ernest Ansermet, CH - 1211 Geneve 4, Switzerland*
[b] *Department of Physics, Osaka University, Machikaneyama-cho 1-1, Toyonaka-shi, Osaka 560-0043, Japan*
[c] *Institute of Science and Engineering, Tokyo Institute of Technology, Ookayama 2-12-1, Meguro-ku, Tokyo 152-8551, Japan*
[d] *Department of Science Education, Kyoto University of Education, Kyoto, 612-8522 Japan*
[e] *Institute of Pure and Applied Sciences, University of Tsukuba, Ibaraki 305-9751,Tsukuba, Japan*
[f] *KEK, High Energy Accelerator Research Organization, Oho 1-1, Tsukuba, Ibaraki 305-0801, Japan*

E-mail: Allan.Clark@cern.ch

ABSTRACT: It is expected that after several years of data-taking, the Large Hadron Collider (LHC) physics programme will be extended to the so-called High-Luminosity LHC, where the instantaneous luminosity will be increased up to $5 \times 10^{34}\,\mathrm{cm}^{-2}\,\mathrm{s}^{-1}$. For the general-purpose ATLAS experiment at the LHC, a complete replacement of its internal tracking detector will be necessary, as the existing detector will not provide the required performance due to the cumulated radiation damage and the increase in the detector occupancy. The baseline layout for the new ATLAS tracker is an all-silicon-based detector, with pixel sensors in the inner layers and silicon micro-strip detectors at intermediate and outer radii. The *super-module (SM)* is an integration concept proposed for the barrel strip region of the future ATLAS tracker, where double-sided stereo silicon micro-strip modules (DSM) are assembled into a low-mass local support (LS) structure. Mechanical aspects of the proposed LS structure are described.

KEYWORDS: Particle tracking detectors; Particle tracking detectors (Solid-state detectors); Si microstrip and pad detectors; Radiation-hard detectors

*Corresponding author.

doi:10.1088/1748-0221/9/04/P04018

Contents

2014 JINST 9 P04018

1 Introduction

The ATLAS experiment [1] is a general purpose detector installed at the CERN Large Hadron Collider (LHC). During 2012, the LHC delivered proton-proton collisions at a centre-of-mass energy of $\sqrt{s} = 8$ TeV, with total integrated and peak luminosities for ATLAS of respectively $\sim$21.7 fb^{-1} and $\sim 7.7 \times 10^{33}\,\mathrm{cm}^{-2}\,\mathrm{s}^{-1}$. A major luminosity upgrade of the LHC (the so-called High Luminosity LHC or HL-LHC) is currently foreseen in the period from late 2022 until 2025. The HL-LHC will deliver a levelled instantaneous luminosity of $5 \times 10^{34}\,\mathrm{cm}^{-2}\,\mathrm{s}^{-1}$ and an integrated luminosity of 3000 fb^{-1} after ten years of operation.

The increased instantaneous and accumulated luminosity foreseen at the HL-LHC will necessitate an upgrade of all major ATLAS detector sub-systems, as well as the trigger and data acquisition. In particular, the replacement of the ATLAS Inner Tracking Detector (ID) will be necessary. The current ID combines high resolution discrete silicon detectors (pixel and micro-strips) at the inner and intermediate layers, with a gaseous straw-tube detector at the largest radii. It is composed of three sub-systems: the Pixel detector, the Semiconductor Tracker (SCT) and the Transition Radiation Tracker (TRT). A central superconducting solenoid magnet surrounding the TRT provides a 2 Tesla solenoidal magnetic field. The ID was designed to operate for ten years at the peak luminosity of $10^{34}\,\mathrm{cm}^{-2}\,\mathrm{s}^{-1}$. Due to the very high track density produced at the HL-LHC,[1] the current ID would suffer from a large increase in both the integrated radiation damage and the detector occupancy, compromising its tracking capabilities beyond an acceptable level [2].

The new ATLAS tracker (Inner Tracking Detector or ITK) is expected to be an all-silicon system with new detector technologies and increased granularity [2, 3]. Its design must ensure radiation hardness, low detector occupancy, low detector material and excellent tracking performance in a high pile-up environment. The ITK baseline layout consists of pixel detectors in the innermost layers and silicon micro-strip detectors at intermediate and outer radii. In the barrel region, at least 4 pixel layers (with a pixel size of 25×150 μm^2 and 50×250 μm^2 in the two inner and two outer pixel layers respectively) are followed by 5 double-sided stereo silicon micro-strip layers. The innermost 3 strip layers consist of *short-strip* sensors (∼24 mm strip length), while *long-strip* sensors (of $\sim$ 48 mm strip length) are used for the two outer layers. The pixel detector extends to a radius R $\sim$ 250 mm, with the innermost layer being located at R $\sim$ 33 mm to be as close as possible to the beam-pipe. The forward region is covered with 6 pixel and 7 strip disks, extending to $|z| \sim 1.7$ m and $|z| \sim 3$ m respectively along the beam direction, with equivalent granularities. This layout ensures an 11 hit coverage in the pseudo-rapidity range of $|\eta| < 2.7$ for interactions within $|z| < 15$ cm.

The baseline integration concept for the barrel micro-strip region is the so-called *stave* concept [4], in which a common mechanical structure integrates the sensors, the electrical lines (service bus) and the cooling circuit. The stave is an ∼1.3 m long object that has a central core composed of a spacing material (carbon-foam or honeycomb) and carbon fiber facings glued on both sides. A service bus for the electrical signals is laminated on top of the facings. Single-sided silicon micro-strip detectors are then glued over the bus and hybrids carrying the front-end electronics are glued on top of the sensitive side of the sensors.

The *Super Module (SM)* is a more conservative back-up barrel integration concept [2] where *Double-sided Silicon Micro-Strip (DSM)* modules are screwed with precision attachments to a light, thermally and mechanically stable carbon fibre *Local Support (LS)* structure. The module is the minimal self-contained detector unit. The heat generated from the front-end electronics is transferred from the DSM module to cooling pipes located in the lateral sides of the LS frame. The LS is designed to hold at least 12 modules, enabling a full coverage in both ϕ and z coordinates. Dead space between adjacent modules is avoided by staggering them along the z-axis. Mechanical and electrical studies have been made to determine the feasibility of this concept.

[1] Assuming a 25 ns bunch-spacing configuration and an instantaneous luminosity of $5 \times 10^{34}\,\mathrm{cm}^{-2}\,\mathrm{s}^{-1}$, the mean number of interactions per crossing is ∼140 with more than 1000 charged tracks per unit rapidity.

2014 JINST 9 P04018

Details of the DSM performance, as well as results from an 8-module electrical SM prototype have been previously presented [5, 6]. This paper describes mechanical design and prototype studies of the SM and its evolution towards a practicable solution for the ATLAS ITK. Together with [6], it summarises the successful completion of a first stage feasibility investigation of the SM concept for the ITK.

In section 2 the main design motivations of the SM are listed. Section 3 then describes the mechanical and thermo-mechanical design, as well as prototype developments, of the light carbon fibre mechanical supports for individual DSM modules. The integration of DSM modules onto the LS is described, and mechanical constraints introduced by the thermal and electrical services are also discussed. Section 4 describes the integration of the SM onto an overall structure. Section 5 describes the expected mechanical and thermo-mechanical performance, in the light of the specifications listed in section 2. Comparisons of these finite element analysis (FEA) studies have been made with prototypes to allow a validation of the FEA, an essential input to future design tuning and development. Section 6 presents a (conservative) estimate of the expected radiation length for the SM structure, including all electrical and mechanical components. Finally, some conclusions are listed in section 7.

2 Design criteria of the silicon strip super module for the ATLAS barrel tracking detector

The Barrel Silicon Strip SM design is based on the demonstrated performance of the existing ATLAS barrel SCT detector [1]. At the same time, the design attempts to address some design short-comings of the existing tracker.

Important features of the existing barrel SCT include the placement accuracy (approximately 60 μm) of individual double-sided modules on 4 concentric carbon fibre barrels [7], and the long-term stability [8] of modules during operation. Stability is maintained at the level of a few μm, with the main alignment shifts after temperature cycling or magnet changes being the overall barrel structure. The SM design aims to maintain or improve on that stability, and as well to retain flexibility for future design optimisations to minimise alignment ambiguities in the radial and z-directions (weak alignment modes). The mechanical design is therefore optimised at every step to separate electrical, mechanical and thermo-mechanical functions, and to minimise thermo-mechanical stresses.

Another important SCT feature that is maintained in the SM design is the choice of individual DSM modules that allow spatially close stereo space point reconstruction, with the axial and stereo sensors separated by at most 300 μm, and the ability (flexibility) to overlap modules if required for alignment and coverage reasons.

Short-comings of the existing ATLAS SCT design include:

- the material budget (X_0) driven mainly by the service material; and
- the disadvantage of mounting individual modules directly on the barrel support structure, making the final assembly and commissioning more complex.

In the SM design, adapted for the LOI layout, the Global Structure (GS) consists of 5 concentric barrels, and in addition a special *stub* layer to maintain tracking acceptance between the barrel

2014 JINST 9 P04018

and forward regions. Rows of individual short-strip or long-strip DSM modules are mounted with a kinematic attachment on a very light, thermally and mechanically stable carbon fibre reinforced polymer (CFRP, see section 3.2) backbone structure called a Local Support (LS). The LS of the barrel layers would hold 13 modules , and the LS of the stub layer would support 2 modules. The LS is the main interface between the modules and the GS. In the current design, each LS would have only 3 kinematic mountings to the barrel, allowing a stress-less end insertion on the barrels and safe handling before insertion. An assembled SM consists of the LS fully loaded with DSM modules, cooling tubes, and electrical services.

The LS design of the SM ensures modularity at each step of the assembly, and largely decouples the design, prototyping, fabrication and both electrical and thermo-mechanical quality control (QA) for the different major elements: the individual modules, the cooling, the LS itself. It allows full re-workability at the individual module level until the final commissioning step and an optimisation of institute resources during all steps of a construction project.

As expanded in following sections, the design philosophy is to maintain build precision and reproducibility on modular components, with minimal mechanical stress and physical movement between components of differing coefficient of thermal expansion (CTE):

- The internal DSM alignment is at the $\pm$ 1 µm level in-plane and is symmetric out-of-plane to minimise intrinsic silicon distortions. The kinematic attachment via a low CTE cooling plate to the LS is with a precision of $\sim \pm$ 10 µm at room temperature;

- The LS is itself fabricated from low CTE CFRP with emphasis on precision and reproducibility. It must be stiff to limit sag following module loading. The LS is itself kinematically mounted with an in-plane precision of $\sim \pm$ 10 µm on a global structure, to minimise thermal stress and to control the global module position following temperature cycling;

- Stresses transmitted from the higher CTE cooling tubes and service buses to the LS and the LS-module cooling interface are minimised.

Compared with an evolution of the existing SCT where individual modules and their services are attached directly to the carbon fibre cylinder, the consequence of using a LS structure may be a slight deterioration of the stability (depending on details of the SM material stiffness and the number of SM mounting points on the barrel) and an increase of the material budget (approximately 0.1% X_0, see sections 3.3 and 6).

3 Local support mechanics for the super module design

3.1 Overview

As noted in section 2, the SM approach involves the assembly of a number of DSM modules on a dedicated carbon fibre LS backbone that is decoupled from the module mechanics and thermo-mechanical behaviour. This section details the LS design, and the step-by-step fabrication and assembly of the LS components.

2014 JINST 9 P04018

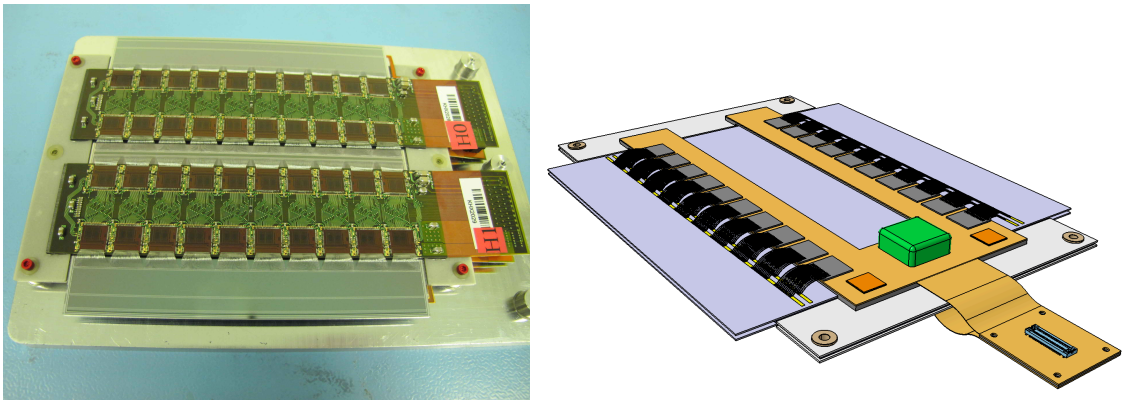

(a) (b)

Figure 1. (a) Photograph of a prototype DSM250 module. (b) The CAD design of the planned DSM130 module using the 256-channel ABCN 130 nm front-end ASIC, attached to the cooling plates and the LS.

Figure 1 (a) shows a photograph of the DSM250 module that has been constructed using the 128-channel ABCN 250 nm CMOS front-end ASIC.[2] Details of the individual module design, as well as the electrical and mechanical performances of the modules, are described in [5, 9–11]. The prototype studies that have been made so far have used this module design. Future prototypes will use DSM130 modules, whose layout is shown in figure 1 (b) and which will use the 256-channel ABCN 130 nm CMOS ASIC now in fabrication.

The DSM module consists of two $\sim 96 \times 96$ mm^2 sensors glued back-to-back on a thermo-pyrolitic-graphite (TPG) baseboard, bridged hybrids holding the ASICS, and two aluminium nitride (AlN) ceramic facing plates at each end of the baseboard. Precision washers accurately position the module to the cooling plates of the LS. To minimise thermo-mechanical distortions the module is symmetrical.

Figure 2 shows the complete 3-D Computer Associated Design (CAD) model of the SM, including the rendering of the DSM130 module, the LS and a service bus along one side and ending with a Super Module Controller (SMC) currently under development. Figure 3 shows how the modules are interfaced with the two longitudinal cooling pipes (shown in grey in figures 2 and 3). Using a rotating assembly stand (section 3.4), successive modules are fixed to the upper and lower sides of these precision Carbon-Carbon (CC2D)[3] cooling plates. The mounting precision of the modules on the LS is determined by the machining accuracy of the cooling plate and fixations. From SCT experience, an in-plane $\pm$ 1 µm precision of the back-to-back sensor positions can be achieved and an in-plane mounting precision (sensor to module fixation, module fixation to cooling plate fixation) at the level of $\pm$ 10 µm can be maintained. The cooling plate fixation to the LS Wings must still be demonstrated.

As with the DSM modules, all prototype studies of the LS have been made using materials appropriate to the study involved, and have been adapted for the DSM250 module design. However,

[2]The DSM modules are designated DSM250 or DSM130 whenever relevant to denote the use of the ABCN 250 nm or ABCN 130 nm front-end CMOS ASIC.

[3]CC2D is a carbon-fibre-epoxy 2-directional ($0^\circ - 90^\circ$) fabric that is fired at high temperature to form a C-C ceramic, with the mechanical strength of carbon-fibre and thermal conductivity of carbon in the plane of the fabric. Supplied by JX Nippon Oil and Energy Corporation, Japan.

2014 JINST 9 P04018

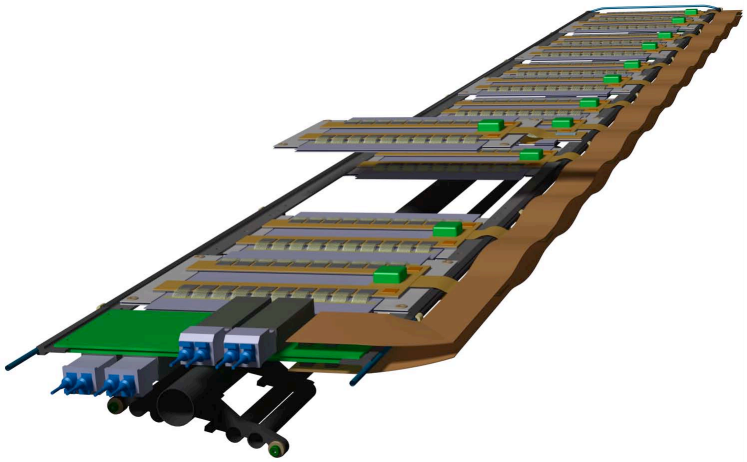

(a)

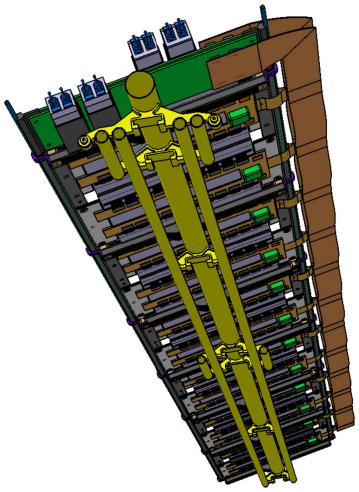

(b)

Figure 2. (a) Top-side CAD views of the SM including the ADCN130 DSM modules, the LS and the Service Bus. One module has been removed to illustrate the connection of the module to the cooling plates. (b) Bottom-side view of the SM. The LS is shown in yellow for clarity.

the CAD models, as well as the finite element analysis (FEA) models, have unless explicitly stated been developed for the DSM130 module.

The module flex associated with each DSM module allows an electrical ground connection to the cooling plate to cope with electromagnetic compatibility (EMI) issues. The module flex has some slack to limit the thermo-mechanical stress and to simplify the assembly procedure, as shown in figure 3 (b). Mechanical issues arising from the services, including EMI concerns, are discussed in section 3.6.

Figure 4 (a) shows the individual components of the LS. The precision LS assembly is made using dedicated jigs fabricated from stabilised aluminium (see section 3.3).The carbon fibre com-

2014 JINST 9 P04018

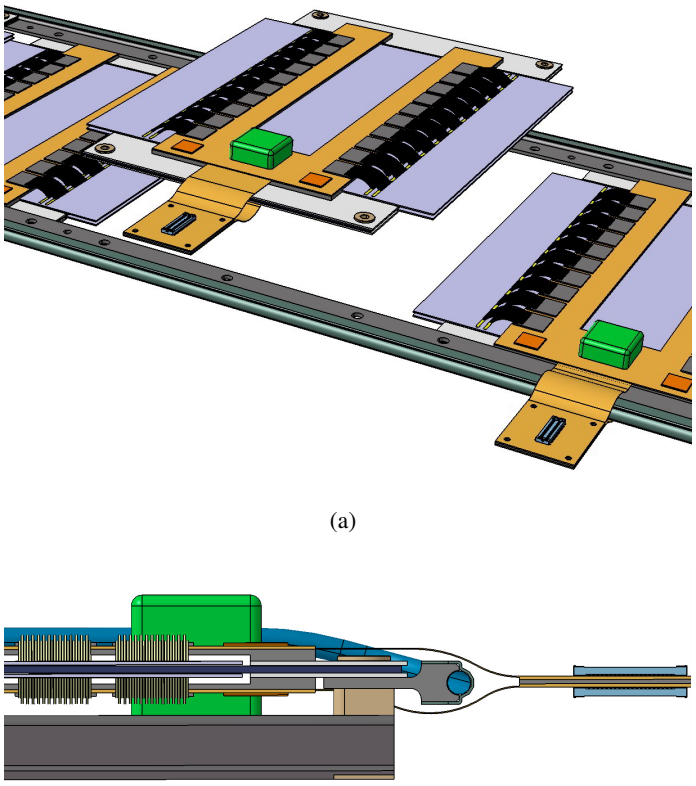

(a)

(b)

Figure 3. (a) Perspective (a) and cross-sectional (b) views of the DSM130 module attachment on the Carbon-Carbon (CC2D) cooling plate and the LS, together in (b) with the electrical module flex grounded to the cooling plate.

ponents[4] are glued using a DP460 epoxy.[5] Figure 4 (b) shows a CAD view of the raw LS with the attached CC2D cooling plates and the cooling pipe, but before the attachment of the modules, service bus and read-out electronics. The cooling plates are positioned with a precision jig and screwed to the wing ends. An important design issue is to maintain CTE matching of the individual components, and to achieve the lowest possible CTE of the assembled LS.

Table 1 lists the individual LS components for the current prototype design. Prototype studies are so far made CFRP layups using T300 fibres.[6] It is expected that significant design optimisation can be achieved following a full comparison of fabricated prototypes with finite element analysis (FEA) models (see section 5).

[4]Carbon Fibre Reinforced Polymer (CFRP) layups are used to simultaneously provide a very stable, light structure that minimises the overall CTE of the LS by using successive layers of different carbon fibre orientation.

[5]Scotch-Weld product, 3M Corporation.

[6]T300 fibres are used for prototype studies. Future prototypes will use M55J fibres. K13C fibres are being considered for high stiffness applications: TORAYCA carbon fibres, Toray Corporation, Japan.

2014 JINST 9 P04018

(a) (b)

Figure 4. (a) Exploded view of the individual Local Support (LS) carbon fibre components, including the 7 carbon fibre reinforced polymer (CFRP) wings, the central support tube and the LS attachments to the Global Structure (GS). (b) CAD design of the CFRP LS structure, including the 7 CFRP wings, the attached Carbon-Carbon (CC2D) cooling plates, the titanium alloy cooling pipes and the attachments to the GS.

Table 1. Components of the current prototype LS structure. A further optimisation of the CFRP material is expected following comparison of prototype results with Finite Element Analysis (FEA) calculations.

Item	**Number**	**Design Details**	**Purpose**
Central Pipe	1	CFRP (T300 fibres, 3 ply layup) Outer Diameter 15 mm Wall thickness < 0.3 mm	Main Support Structure
Interface blocks	3	PEEK loaded with carbon fibre and CNC machining	LS end-insertion attachment
Full length lateral pipes	2	CFRP (T300 fibres, 3 ply layup) Outer diameter < 6 mm Wall thickness < 0.3 mm	Guiding tubes for insertable locking tool
Short length lateral pipes	6	CFRP (T300 fibres, 3 ply layup) Outer diameter < 6 mm Wall thickness < 0.3 mm	Guiding tubes for insertable locking tool
Cooling plate	2 x 3	Carbon-Carbon (CC2D) segments	Machined plate to house cooling pipe and provide precision module attachment
Cooling plate facing	2 x 1	CFRP (T300 fibres, 3 ply layup)	Maintain integrity of cooling pipe contact to cooling plate
Wing	7	CFRP (T300 fibres, 2 layer fabric)	Cross-beams to support modules

2014 JINST 9 P04018

Table 2. Component dimensions and material of the current wing design.

Part	Material	Design Details	Comments
Facing	CFRP (2 layer T300 fabric)	400 µm thickness	Each fabric layer is a 2 ply T300 layup with fibre orientation $(0°, 90°)$ Tests also made with single layer fabric
End Pieces	PEEK 1000	Envelope requirement is < 6 mm height	Glued to the facing using DP460

Figure 5. Upper and lower views of a prototype CFRP layup wing for the LS, including PEEK1000 attachments at the wing ends.

3.2 Design and fabrication of Carbon Fibre Reinforced Polymer (CFRP) wings for the local support

The CFRP Wings shown in figure 4 are an essential part of the LS system, as they hold the cooling plate segments in a precise and stable position. The shape and number of wings is optimised using FEA studies to minimise the total LS and SM material, while retaining an acceptably small SM deformation after the loading of all modules on the LS (see table 2 and section 5). Figure 5 shows the photograph of a prototype wing, after the glueing of small PEEK 1000 extremity pieces.

The prototype wing has been developed in collaboration with Composite Design S.A.[7] Particular attention has been made to verify the design and fabrication of the wing: issues include the precision and stability after machining of the attachment to the central support tube, and the carbon fibre integrity for very small bending radius. Dedicated aluminium moulds have been fabricated to ensure the correct mechanical features. The moulds are initially used for the layup wrapping and moulding. Using precision numeric (CNC) machine tools, the moulded wings are then contoured, glued at each end with PEEK1000 reference pieces and precision machined. At each step, jigs are used to maintain the planarity and to ensure the accuracy of the PEEK reference points. The full fabrication and machining process can be industrialised.

3.3 Precision assembly of the local support

The LS assembly uses a precision jig made from stabilised cast aluminium (AW-5083) to limit stress relief and resulting deformations after machining. The final assembled precision is therefore largely unaffected by the precision of component pieces.

[7] Composite Design S.A., Crissier, Switzerland.

2014 JINST 9 P04018

A jig of approximately 1300 mm length was initially fabricated in industry to study the insertion of assembled SM units on a cylindrical structure. The maximum in-plane and out-of-plane distortion of this jig was measured to be 20 µm. A second prototype jig of approximately 1250 mm length was then fabricated to assemble the LS, with the same specifications and vendor. The wings when assembled onto the central pipe are expected to be planar with the same tolerance since it is determined by the jig machining precision as noted above. In future LS developments, the planarity will be measured using the end-of-wing PEEK reference points.

A *demonstrator* prototype has been used to verify the successive assembly steps of the LS, as well as the insertion of a LS onto a cylindrical structure. Figures 6 and 7 show the successive assembly steps for the LS prototype:

- Figure 6 (a) shows the main assembly jig for the LS. In this initial step, the small diameter CFRP tubes are laid in the jig and glued to lateral supports. The main CFRP support tube is temporarily replaced by a heavy steel rod of the same outer diameter to maintain the component accuracy during polymerisation;
- Figure 6 (b) shows the second step when the central CFRP tube is positioned and glued on the structure;
- The jig is then inverted to organise the wing assembly, as shown in figure 6 (c). Some additional blocks are used to position the wings by defining a reference plane with respect to the global structure. These are the parts that fix the LS onto the barrel, and which provide the tilt angle of the LS; and
- The last operation on the LS assembly is to position and glue the locking mechanism when the LS is attached to a global support (the prototype studies have assumed locking at 3 different positions along the LS length, see section 4.3).

Figure 7 shows the resulting LS backbone on its jig, in this case an assembled LS prototype. The LS is then ready to be equipped with cooling plates and their associated cooling tubes and CFRP facings, the necessary DSM modules, and the service bus. All of these items can be tested independently of the LS, and can be replaced on the LS at any stage for QA reasons.

The LS support fabrication uses a controlled amount of glue, determined by the jigs. This is important to minimise possible ageing concerns, to ensure uniformity of the material budget between different LS units, and to ensure the uniformity of mechanical and thermo-mechanical behaviour during large-scale production.

The total material budget of the LS, averaged over the active area of the SM, is estimated to be 0.18% X_0 (see section 6). The total material budget per barrel layer could be reduced by approximately 0.1% X_0 if the removable end-insertion LS baseline were not retained (see section 2).

As with other design aspects, there is an incremental effort to further reduce the material of both the wing and central pipe. Recent single layer CFRP wing prototypes are promising and in addition reduce the cost (the wrapping and co-curing is made in a single step). The same approach will be investigated for the central CFRP pipe in an effort to further reduce the wall thickness. However, any material gain, small compared to the expected service material, must take into account stringent short-term and long-term stability requirements. Furthermore, the CTE of the central CFRP pipe determines the in-plane movement of loaded modules with respect to a global fiducial point during temperature cycling and the CTE must therefore be minimised.

2014 JINST 9 P04018

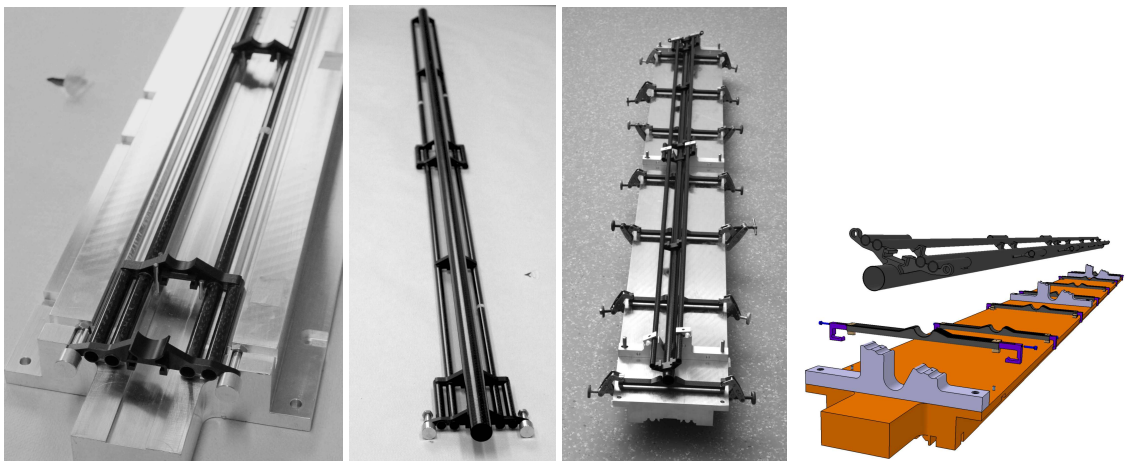

(a) (b) (c) (d)

Figure 6. (a) Top side of aluminium LS assembly jig, machined using AW5083 cast aluminium, before placement of the central CFRP support tube. (b) Photograph of the assembled LS, after attaching the CFRP support tube but before attaching the wings. (c) Bottom side of the jig used for wing assembly including 3 aluminium blocks that determine the azimuthal tilt angle when attached to the barrel support. (d) Schematic 3D CAD drawing of (c).

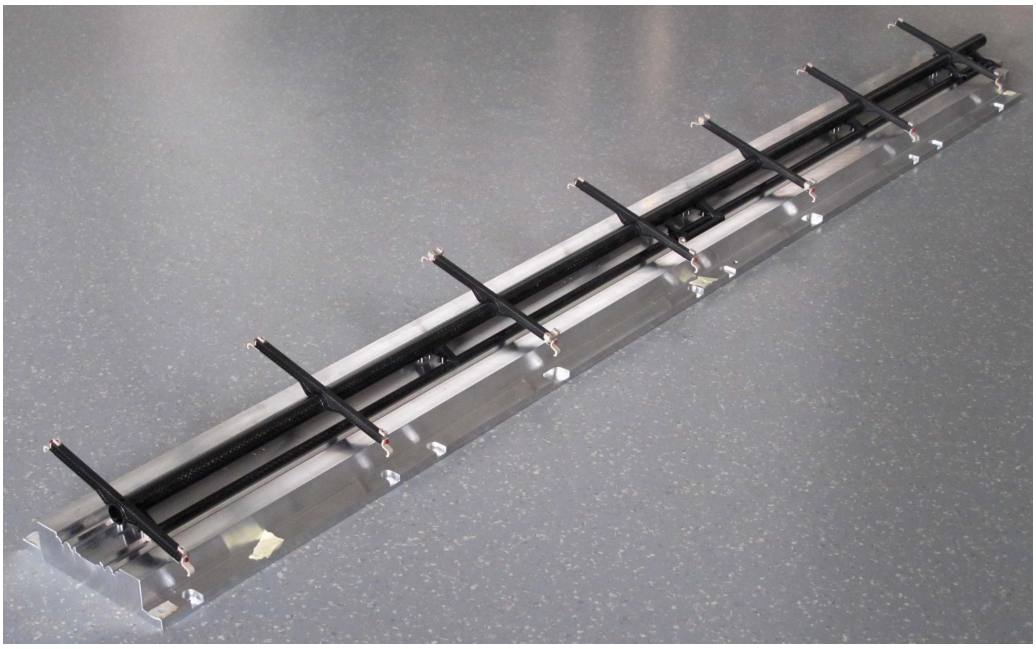

Figure 7. Photograph of the fully assembled CFRP backbone LS on its jig, before being equipped with the cooling plates, service bus and DSM modules.

2014 JINST 9 P04018

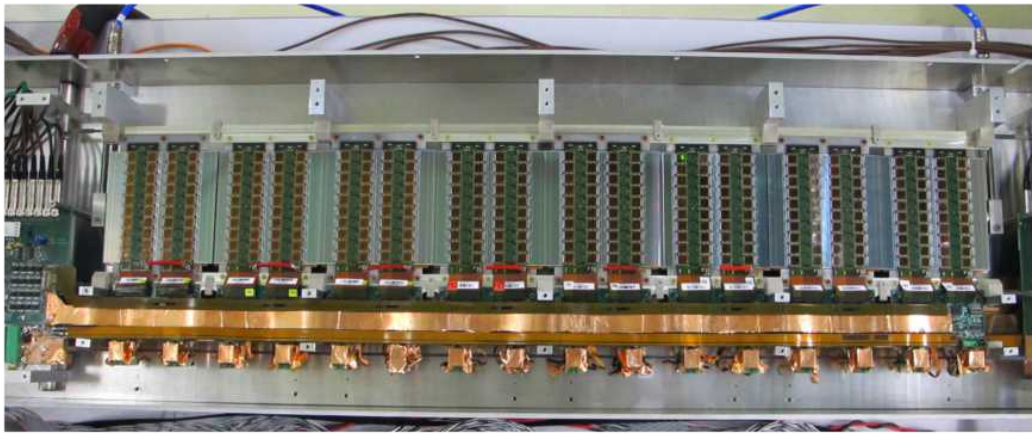

Figure 8. Photograph of the 8-module electrical prototype SM described in reference [6].

3.4 Interface of modules on a local support of the super module

The assembly procedure of modules onto the LS has been fully tested using prototype DSM250 modules and aluminium cooling plates on the simplified 8-module electrical SM [9] shown in figure 8. It has also been tested with a 12-module aluminium LS loaded with dummy mechanical modules. In successive steps:

- Modules are attached using a precision jig to the upper surface of a cooling plate on each side of the module. The DSM130 design has 2 module fixation points on the module and it is expected on the basis of FEA studies that 3 of the fixations will be kinematic slots (see section 5);
- The jig is rotated and additional modules are attached to the lower surface of the cooling plate.
- After the cooling plates are fully populated and tested in the jig, the modules and cooling plates are transferred as a single entity from the stabilised aluminium jig onto the LS. A handling jig will be developed for this step. The SM modularity is clearly emphasised; in the case of faulty parts on a module, the complete module assembly can be easily re-transferred to the handling jig for re-work without delicate operations on the LS.

3.5 Constraints from cooling requirements on the LS mechanical design

Separate heat paths from the module hybrid and module sensors [5, 9] transfer the heat to the high thermal conductivity cooling plates that are mounted on the LS. These cooling plates also serve as the precision mounting for the modules (sections 3.1 and 3.4). The thermal performance is further discussed in section 5.

The mechanics of the cooling system includes the cooling plates, the cooling pipes, and the thermo-mechanical contact between them, as well as the precision mounting of the cooling plates on the LS backbone. The cooling system design includes the following features:

2014 JINST 9 P04018

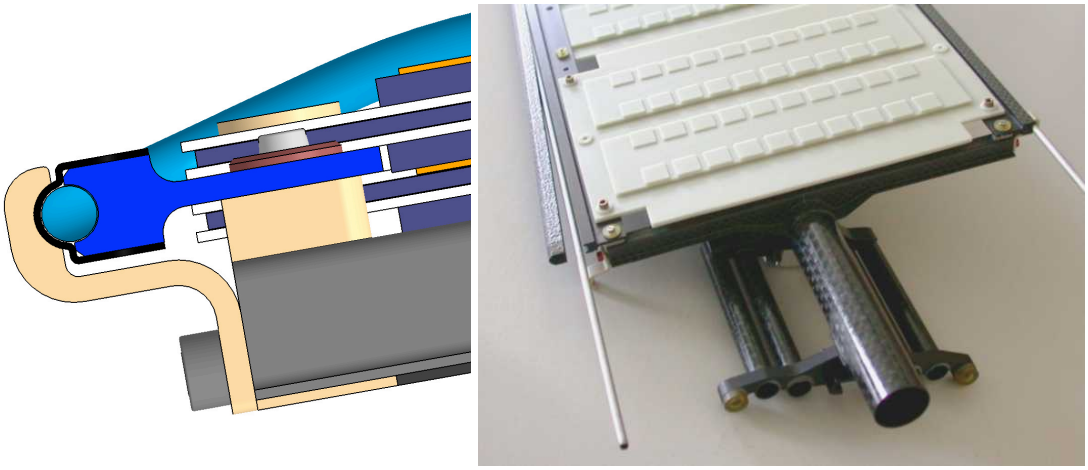

(a) (b)

Figure 9. (a) A simplified cross section of the SM cooling plate together with the cooling pipe that is kept in contact with the plate by the facing plate and thermally conductive grease. (b) The cooling plate (in this case aluminium) mounted on a fully assembled prototype LS. A dummy mechanical DSM module is attached to the cooling pipe.

- The cooling system is mechanically independent of the LS, allowing for the independent design and prototyping of the cooling plates and pipes (including if necessary changes to the pipe diameter or composition, the coolant, etc.), and re-workability during successive quality control steps;
- The precision machined cooling plates are fabricated from CC2D. After loading with DSM modules, the plates are screwed on the precision PEEK pads of the LS wings; and
- To ensure minimal mechanical stress due to the CTEs of the cooling plate and the cooling pipes, the pipes move longitudinally within the cooling plate while maintaining good thermal contact using conductive grease (the principle used in the existing barrel SCT [1, 8]).

Figure 9 (a) shows a simplified CAD cross-section schematic of the cooling plate. The photograph of figure 9 (b) of an early SM mechanical prototype shows how the cooling pipe is inserted and maintained within the cooling plate. In the current design, there are 3 CC2D cooling plates on each side of the LS because of the limited available length of CC2D blocks. Full-length cooling plates using CC2D (from a dedicated production run) or other CFRP materials with equivalent thermal and mechanical properties are being considered for improved mechanical stability (see section 5.3). As already noted, the foreseen mounting precision ($\pm$ 10 µm) of the cooling plates onto the LS Wings must still be demonstrated.

The baseline CO_2 coolant uses a 2.0 mm inner diameter titanium alloy pipe. However, the design allows changes to this baseline independently of the modules and LS. The high CO_2 Heat Transfer Coefficient (HTC > 8000 Wm^{-2} $^oK^{-1}$) as compared to other coolants (for example C_3F_8) ensures excellent heat transfer from each sensor and hybrid of the SM.

Figure 10 shows the first CC2D prototype of the cooling plate. The full machining and assembly of the cooling system has been validated using this prototype. The 2-dimensional in-plane

2014 JINST 9 P04018

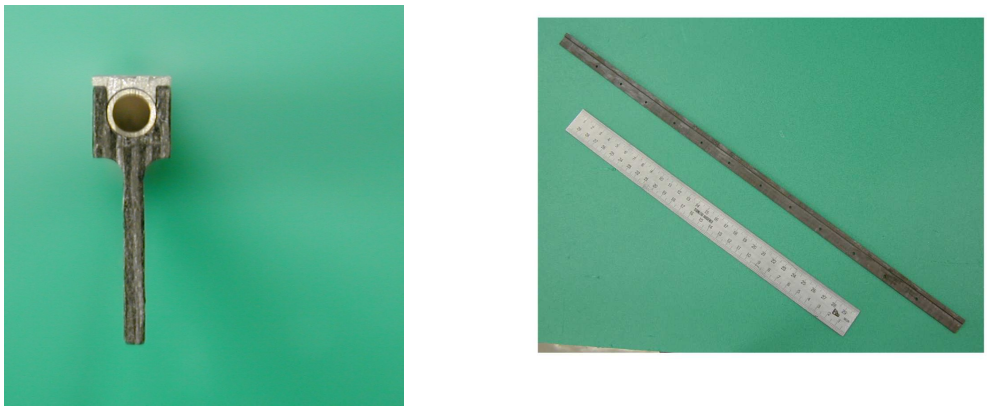

(a) (b)

Figure 10. Cross-sectional photograph of a prototype CC2D cooling plate, following machining. The cooling plate design and pipe diameter have evolved slightly following this prototype. (b) Longitudinal view of the same cooling plate. The ruler length is 30 cm.

CTE of CC2D is close to that of the fibre lay-up in-plane (-0.8 ppm $^0K^{-1}$) and to that of the filler out-of-plane (10 ppm $^0K^{-1}$). Therefore, there is no mechanical stress resulting from the differing CTEs of the cooling plate and the titanium alloy cooling pipe apart from the grease viscosity.

The high conductivty thermal grease interface plays a crucial role, both mechanically and thermally. The thermal path between the module facings and the cooling plate is ensured by the thermal grease to fill the air gaps due to surface imperfections. Since the thermal resistance of the latter depends on the layer thickness it must be thin (less than 50 µm) and optimised to compensate for planarity or roughness defects on the two contact surfaces. A nominal 50 µm thermal grease layer is also required between the cooling pipe and the cooling plate, allowing for assembly and for the pipe expansion and contraction when the temperature conditions are changed. The thermal grease must maintain its performance throughout the operational lifetime of the HL-LHC, following the effects of ageing as well as the maximum expected integrated 1 MeV equivalent neutron fluence of 8.1×10^{14} $n_{eq}cm^{-2}$ and ionising dose of 288 kGy [2, 12].

A number of candidate greases have been thermally and mechanically evaluated [13, 14] independently of manufacturer data, in the context of both this and the ATLAS IBL [14] projects. On the basis of dispensing control (viscosity), stability following sustained thermal cycling and the measured thermal conductivity, the non-silicone, ZnO-filled HTCP grease has been retained at this stage.[8] It is also used for the IBL project. For DSM modules using the ABCN 130 nm ASIC (1 mW per channel), the mean module temperature increase due to the thermal grease is expected to be 0.6 ^oC. The evaluation of candidate greases remains an important future activity.

Several thermal grease samples, including HTCP, have been irradiated to an equivalent 1 MeV neutron dose of 10^{15} $n_{eq}cm^{-2}$ and beyond using the 24 GeV PS T7 proton beam at CERN. Fol-

[8]Electrotube, Ashby de la Zouch, United Kingdom. See www.electrotube.com.

2014 JINST 9 P04018

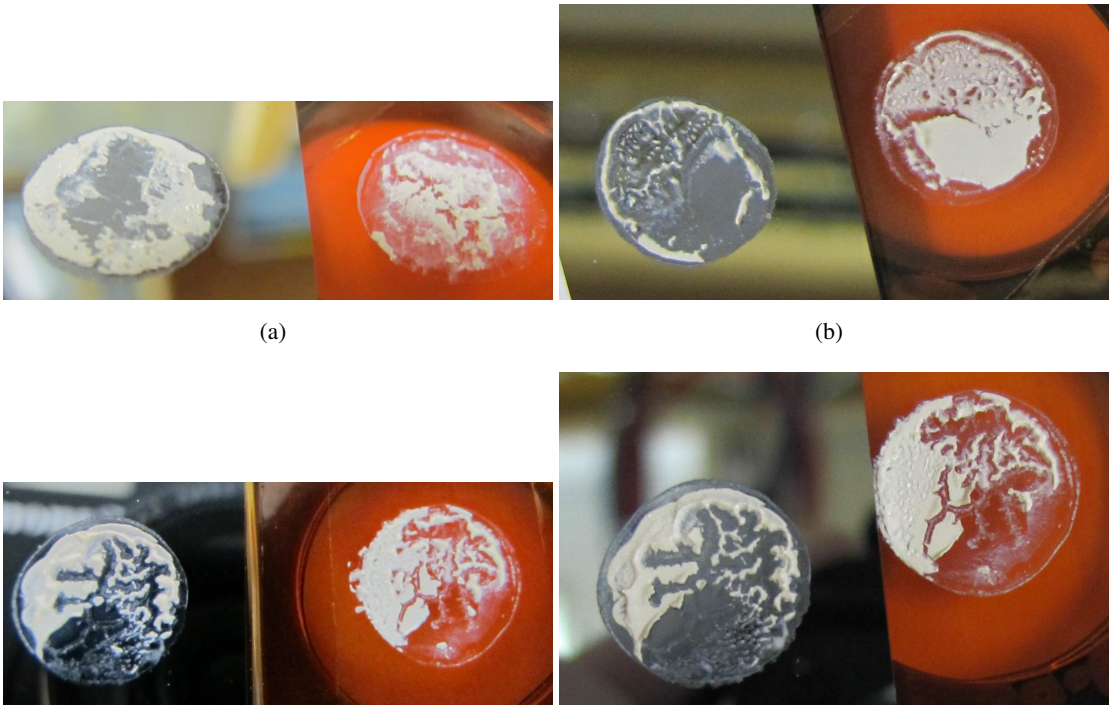

(a) (b)

(c) (d)

Figure 11. Photographs of the HTCP compound. Each sample is a disk of 10 mm diameter and 50 µm thickness sandwiched between a silicon and a kapton surface. The photographs are made after opening the 2 surfaces following irradiation: (a) irradiation to a fluence of 10^{15}n$_{eq}$cm^{-2}, (b) irradiation to a fluence of 2×10^{15} n$_{eq}$ cm^{-2}, (c) irradiation to a fluence of 2×10^{15} n$_{eq}$cm^{-2} with subsequent ageing over a 10 month period at room temperature in a normal atmosphere and (d) irradiation to a fluence of 5×10^{15} n$_{eq}$cm^{-2}.

lowing this dose, the thermal conductivity deteriorated ($\sim 30\%$) due mainly to a reduction of the contact surface, but the compound remained sticky. Additional samples that were irradiated at 5 times the expected HL-LHC strip fluence became somewhat plaster-like in consistency, but still acceptable. Nevertheless some ageing concerns persist for this compound. Figure 11 shows the result after irradiation and ageing of several HTCP samples (a disk of 10 mm diameter and 50 µm thickness sandwiched between a silicon and a kapton surface):

(a) following irradiation to a fluence of 10^{15}n$_{eq}$cm^{-2};

(b) following irradiation to a fluence of 2×10^{15}n$_{eq}$cm^{-2};

(c) following irradiation to a fluence of 2×10^{15}n$_{eq}$cm^{-2} and subsequently a 10 month ageing period at room temperature and normal atmosphere; and

(d) following irradiation to a fluence of 5×10^{15}n$_{eq}$cm^{-2}.

It is believed that, following irradiation and ageing, the compounds become much dryer and that part of the original volume is lost by evaporation. This indicates the need to continue large scale in situ ageing tests of irradiated samples and to characterise other grease candidates.

2014 JINST 9 P04018

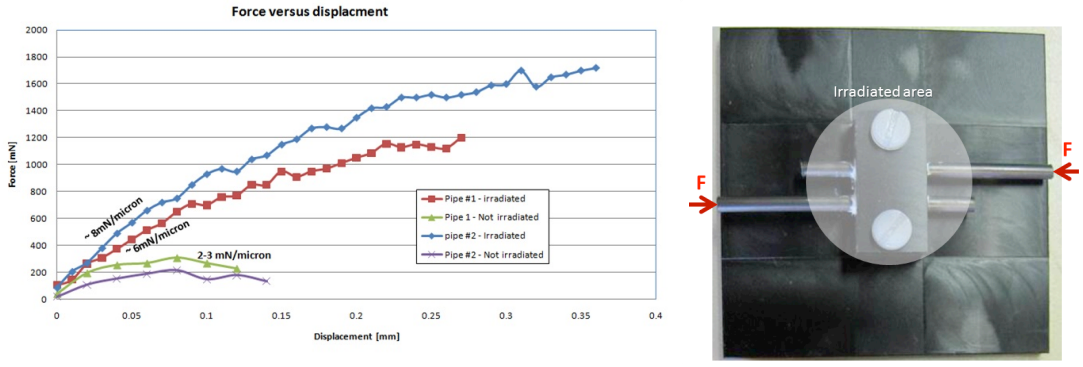

(a) (b)

Figure 12. Measurement of the displacement as a function of the applied force (a) for cooling pipes inserted into a dummy cooling plate (b), using both irradiated (10^{15} n_{eq} cm^{-2}) and non-irradiated grease samples.

The mechanical properties following irradiation have been evaluated by a measurement of the equivalent elastic modulus (Young modulus). As shown in figure 12, the Young modulus of several HTCP samples have been measured following irradiation to 10^{15} $n_{eq}cm^{-2}$. From the measurements, a conservative estimate of the equivalent Young modulus is made (it maximizes the effect of the grease on the thermo-mechanical stresses). Before and after irradiation, the Young modulus changes from 90 Mpa to 230 Mpa. This measurement has been used as input to FEA calculations that are described in section 5.

In conclusion, the mechanical and thermal integrity of the cooling system has been demonstrated. Further FEA studies described in section 5 confirm that the specifications on thermal stress can be met. Continued studies on the choice of a high thermal conductivity grease remain important. The system design can be refined until late in the prototype stage.

3.6 Constraints from electronic service requirements on the LS mechanical design

This section presents a short overview of the electronic services and their implication for the LS mechanics. Figure 13 shows a 3D CAD rendition of the SM, adapted for DSM130 modules, and including the service bus as currently foreseen for the electrical SM prototype [6, 9] as well as the SM Controller (SMC) at the end of each SM with the ABCN 130 nm CMOS ASIC. Neither unit has been optimised at this stage. Figure 8 shows the service bus and SMC board as implemented on the electrical SM prototype using DSM250 module prototypes.

The service bus and SMC development has primarily been to demonstrate the electrical feasibility of the SM design and further design work is required for compatibility with future DSM130 modules, as well as the Hybrid Controller Chip (HCC)[9] [15] being developed in 130 nm CMOS technology and the future SMC board at the end of each SM. Furthermore space constraints are imposed by the overall tracker layout.

The SMC board will serve both mechanical and electrical functions. Mechanically, it will serve as the termination of the lateral service bus, and for all service connections (cooling, DAQ,

[9]The HCC is an ASIC being developed in 130 nm CMOS technology to serve as the interface between the service bus and the ABCN 130 readout ASICs mounted on the hybrid

2014 JINST 9 P04018

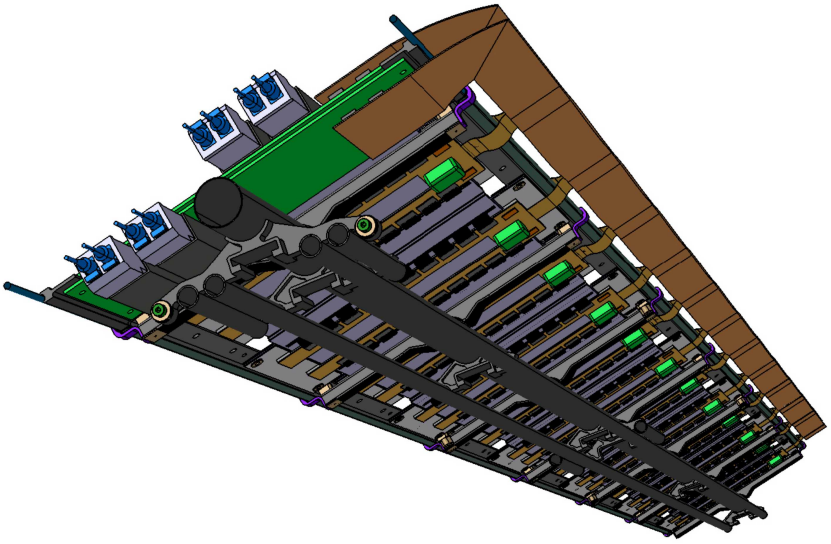

Figure 13. CAD model of the DSM130 module prototype installed including the Super Module (SM) Controller module (SMC) at the end of the SM.

low-voltage and high-voltage connectors, and opto-electric converters). The length of the SMC will be minimised to limit the space between the last active barrel module and the first active disk module. It will also take into account the space needed to organise the services (in particular the bending radii of the cooling lines and services).

The DSM module readout will be powered by either serial powering or on-hybrid DC-DC converters.[10] The sensor bias voltage will be also multiplexed.

While having the significant advantage of reducing the material budget for the services, this introduces a new constraint in terms of electromagnetic interference (EMI), in particular for the DC-DC converter option. The module flex associated with each module[11] allows a ground connection to the cooling plate in order to cope with EMI issues. The small size and the high efficiency of such a DC-DC converter is obtained at a high pulse width modulation (PWM) carrier frequency of 2 MHz, introducing harmonics up to 200 MHz and causing EMI in the modules. Particular attention must be paid when designing the module and structure to reduce the common mode noise induced by EMI, by providing a good shielding and optimal filtering of the DC-DC converter, providing adequate shielding and grounding for the service bus, and draining the common mode noise with a good ground connection.

These 3 requirements are being implemented in the mechanical and module design:

- The DC-DC converter will be covered. It will be directly soldered to the hybrid flex and any common mode noise will be drained by the ground plane rather than passing through a connector;

[10] The choices of high-voltage (HV) and low-voltage (LV) powering options have not been made. In the case of LV powering, both serial powering and DC-DC converters are being considered, and the design can be adapted accordingly. In the prototype studies, the DC-DC option is used.

[11] The module flex will have some slack to limit the thermo-mechanical stress and to simplify the assembly procedure (tolerance).

2014 JINST 9 P04018

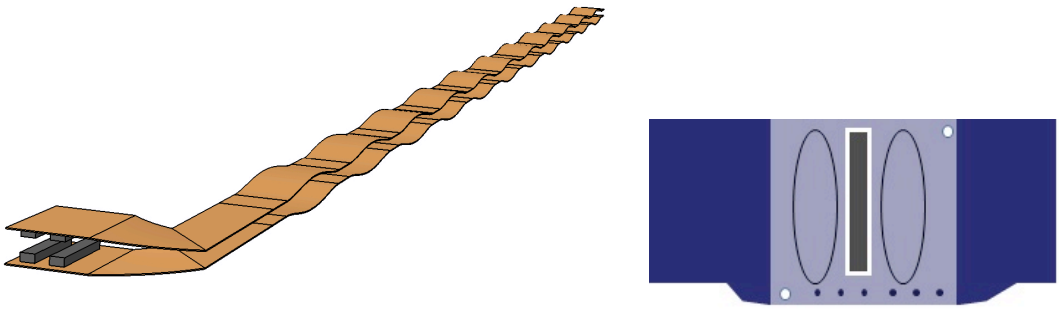

(a) (b)

Figure 14. (a) Service bus layout schematic foreseen for modules using the ABCN130 front-end chip. (b) Expected reinforcement in the connector region with a 300 µm thick stiffener to connect to the module pigtail.

- The hybrid has a common analog and digital ground plane and will be electrically connected to the cooling plate that will reinforce the equipotential of the modules on the LS. The module TPG baseboard will be connected to the high voltage of the sensor back plane, therefore being a 'virtual ground', or will be floated;

- The detector backplane is sensitive to EMI and must by AC connected to the hybrid ground plane through at least 4 bypass capacitors located at each corner to ensure a good equipotential;

- The service bus flex will contain at least one ground plane acting as a shield for its internal signals and improving also the common mode noise drain;

- The SMC ground plane will be connected to the same electrical reference (service bus, end of cooling plates);

- The end of the SM will be electrically connected to the end barrel flange and bonded to the global earth of ATLAS for a good common noise drain.

The future prototype service bus layout (figure 14) will be based on that of the IBL stave flex [14]. The existing service bus design assumes a 20 mm width, excepting the connector region (22 mm) to allow for low voltage vias and interconnections between the Al and Cu substrates. The two 50 µm thick Al layers will be tapered between 11 mm and 20 mm in width. The Cu layers will consist of two 15 µm thick layers to carry the LVDS, HV and DCS signals, and one 5 µm thick Cu mesh to control the LVDS impedance. Averaged over the SM active area, the service material budget is expected to be 0.11 % X_0 (section 6), including the stiffener used at the pigtail connector for individual modules.

2014 JINST 9 P04018

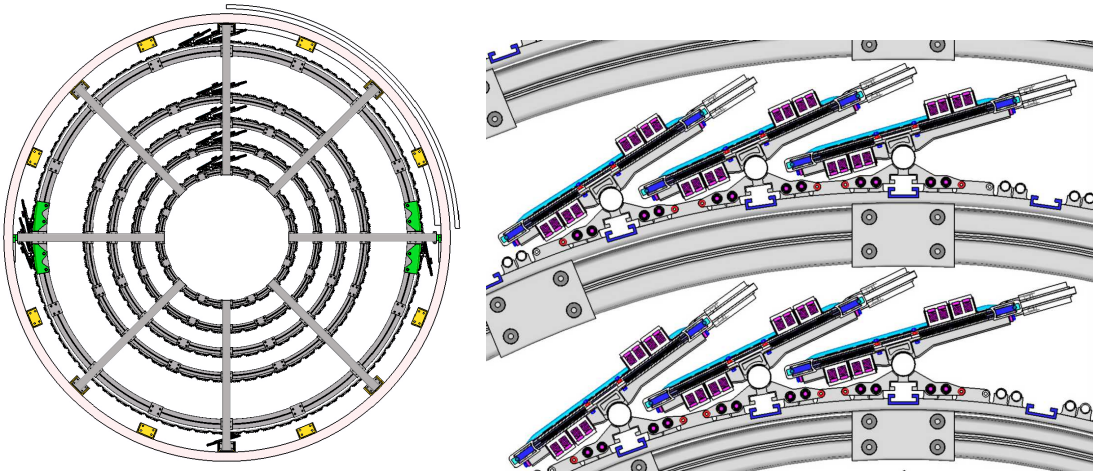

(a) (b)

Figure 15. (a) Cross-section CAD view of the Barrel Global Structure as foreseen in [2], including the inserted LS in all layers, and an initial GS interlink design. (b) Detailed CAD view of adjacent SM units inserted in the GS.

4 Interface of the super module with the global structure

4.1 Overview

In the current LOI design [2] the barrel Global Support (GS) consists of 5 concentric carbon fibre barrels of nominal active radius $407 < R < 1000$ mm, and half-length 1275 mm. In addition, a *stub* layer consisting of 2 modules will exist at nominal active radius $R = 862$ mm and in the longitudinal range $1079 < z < 1275$ mm. The cylinders will be interlinked with 8 precision carbon fibre support legs, much as for the existing SCT, as illustrated in figure 15 .

The GS will be assembled and checked for metrology prior to attaching the SM units. This allows the independent development and fabrication of the GS and LS, and allows an intermediate commissioning step of the modules on each SM. It is the major reason for developing the LS strategy, and in particular the LS stress-free end insertion technique noted in section 4.3. The consequence is an increase in the required radial space, and additional material ($\sim 0.1\ X_0$). The interfaces to the GS are of two kinds: the 3 locking points (section 4.2); and the geometrical interference with the Interlinks (an interlink must be removed to insert some SM units without affecting the GS stability, see section 4.3).

4.2 Locking points on the global structure

The LS design adapted to the SM currently foresees 3 fixation points over the SM length. These are located at $z = 0$ mm (nominally kinematic to allow for longitudinal sliding), at $z \sim 600$ mm (also nominally kinematic to allow for longitudinal sliding), and in the vicinity of the SMC at $z \sim 1200$ mm (where all the degrees of freedom are fixed using precision positioned pins and screws). Clamping in the vicinity of the SMC is essential because of other assembly operations, including electrical and cooling service connections that might introduce mechanical stress. The longitudinal sliding on the two other fixation points prevents stresses that could be introduced in

2014 JINST 9 P04018

the SM by GS movements or by small CTE mismatches between the LS and GS structures (both structures have minimal CTE).

Figure 16 (a) shows the nominal positions of the 3 fixation points that are mounted on reinforced CFRP rings. The locking mechanism at $z = 0$ mm allows a gap-free overlap of silicon sensors for longitudinally adjacent local supports. The fixation points are shown on a SM prototype in figure 16 (b).

The sliding joints at $z = 0$ mm and $z \sim 600$ mm are fabricated using PEEK 1000. Machined male and female cone shapes dock in position, allowing for possible initial misalignments during SM insertion of up to ± 1 mm. Once docked in position, the male and female cones can freely slide in an interface attached to the barrel reinforcing rings. There are 2 joints at each location, designed to prevent the LS from rotating around its longitudinal axis.

Figure 17 shows a close-up perspective detail for the sliding $z = 0$ mm (a) and $z = 600$ mm (b) locking points, as well as the fixed locking point at $z = 1200$ mm.

The robustness and reliability of the design has been demonstrated using a full-scale mock-up (the prototype LS of the SM supported on a dummy plexiglass GS) as discussed in section 4.3 and shown in figure 16 (b). Figure 17 (d) shows the prototype locking structure at $z = 0$. The FEA calculations discussed in section 5 include the mechanical behaviour of the 3 fixation points including the proper degree of freedom (clamping and sliding), as well as the influence of loading the SM with modules and services and the effect of position on the GS.

4.3 The end insertion mechanism

The design of the end insertion has been successfully prototyped using the prototype SM and the LS noted above. The design allows stress-free insertion and fixation, and independence from the required SM orientation for both insertion and removal. It also allows safe handling outside the GS (for example quality assurance prior to insertion, or repairs during commissioning). The following CAD schematics illustrate the different steps to insert the SM into the GS. Figure 18 shows the SM as it is handled in an aluminium frame attached to the LS before insertion. This frame also serves as one of 2 temporary sliding backbones during insertion or removal. Figure 16 (b) shows the SM envelope after insertion.

As shown in figures 18 and 19, the SM and LS is inserted as follows:

- A small aluminium bracket is temporarily fixed in front of the SM barrel location;
- The first backbone is inserted into the future SM position on the barrel and clamped at the bracket; the SM with its handling backbone is aligned and clamped to the bracket;
- The SM and its backbone are released and allowed to slide along the 2 backbones up to a mechanical stop provided by the $z \sim 1200$ mm location; this is a stress-free transfer between the backbones;
- The $z \sim 1200$ mm fixation is locked in position to provide a z-reference and the SM backbone is then removed;
- The $z = 0$ mm and $z \sim 600$ mm fixations are locked into place using a long screwdriver tool passing through the short lateral guiding tubes of the LS;

2014 JINST 9 P04018

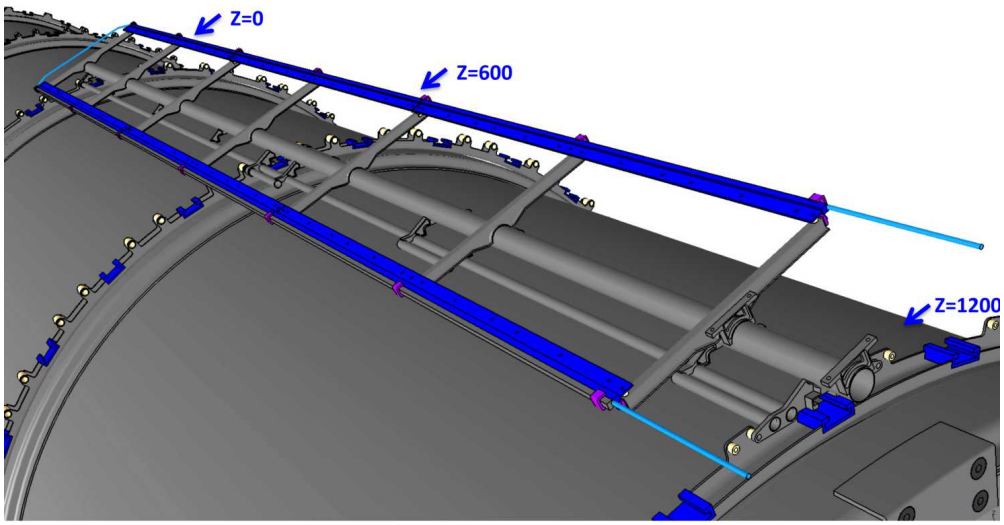

(a)

(b)

Figure 16. (a) CAD model of a LS on a barrel with the attachment points at 3 points along the LS length. The attached modules are not shown for clarity. A second LS is loaded from the other end of the support barrel and is designed to allow a gap-free overlap of the silicon sensors at z = 0. (b) The prototype CFRP SM, loaded with dummy DSM250 modules of the same external dimensions as the prototypes, attached on a cylinder (GS) after attachment to demonstrate the stress-free locking procedure for the SM prototype.

2014 JINST 9 P04018

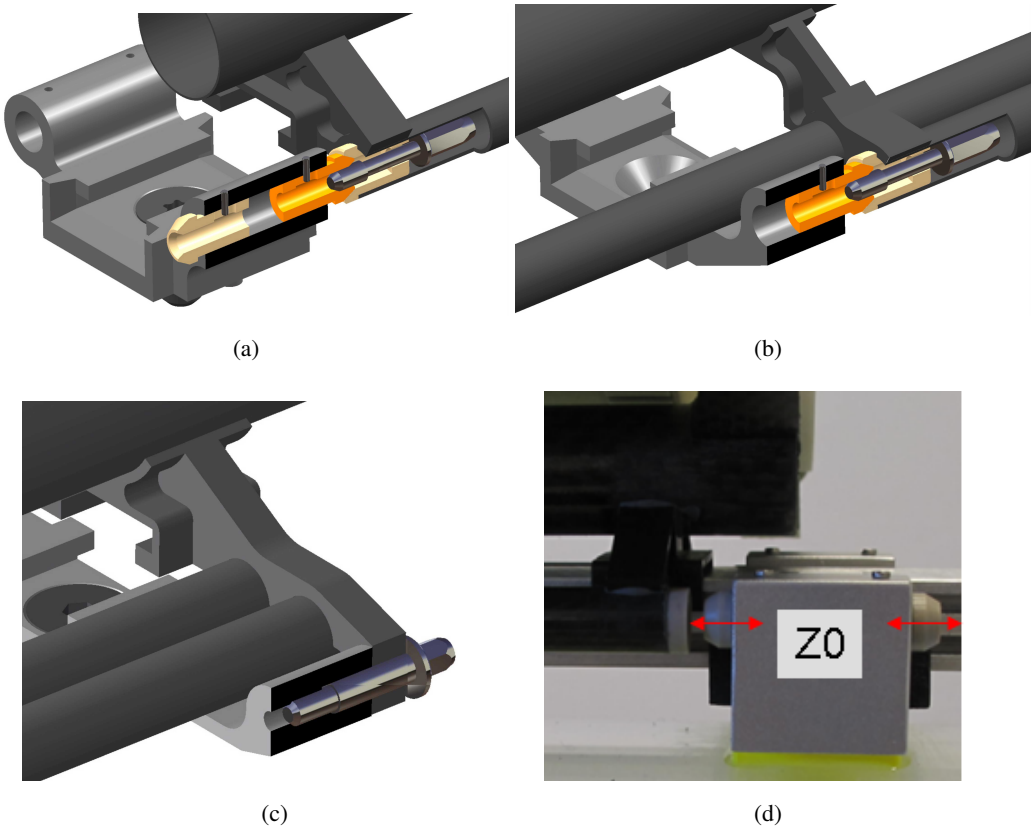

(a) (b)

(c) (d)

Figure 17. Perspective CAD drawings of the stress-less sliding locking points for attachment of the LS to the GS at (a) z = 0 (a) and (b) z = 600 mm. A perspective of the the fixed locking point at z = 1200 mm is shown in (c). A prototype of the sliding attachment point at z = 0 is shown in (d).

- Finally the remaining aluminium backbone is removed. The procedure can be reversed to remove a SM. In some cases one interlink must be removed to enable access for the SM; in that case, possible complications due to the service connections must still be understood.

Figures 19 (a), (b) and (c) summarise the insertion method and the locking mechanism using the prototype barrel and prototype mechanical SM with dummy DSM modules noted previously. The prototype barrel is a transparent plexiglass cylinder with the relevant features added (the 3 locking points, and the bracket fixation). Figure 19 (a) shows the SM placed on the removable aluminium back-bone before insertion. In (b) the SM is shown after being slid into place but before locking. The locking mechanism at z = 0 is clearly visible. In (c) and (d), a long screwdriver is guided by the small cylindrical tubes on the LS to lock the fixations at z = 0 and z = 600 mm.

In conclusion, the SM end insertion technique and the related locking points are simple and effective. Some fine-tuning (for example the backbone shape and material, as well as the end bracket design) is still required, but the design is fully validated using the demonstrator LS as detailed in figures 18 and 19.

2014 JINST 9 P04018

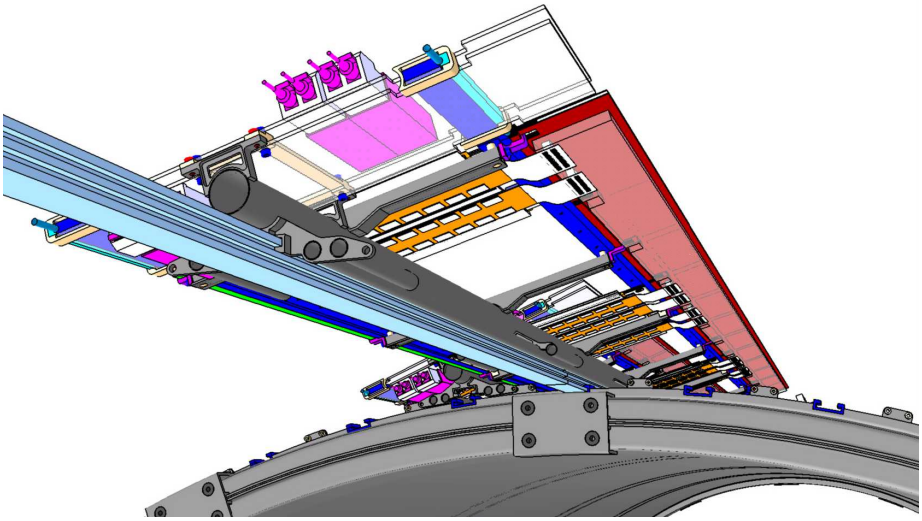

Figure 18. CAD model of a SM on a removable backbone rail being inserted into the GS.

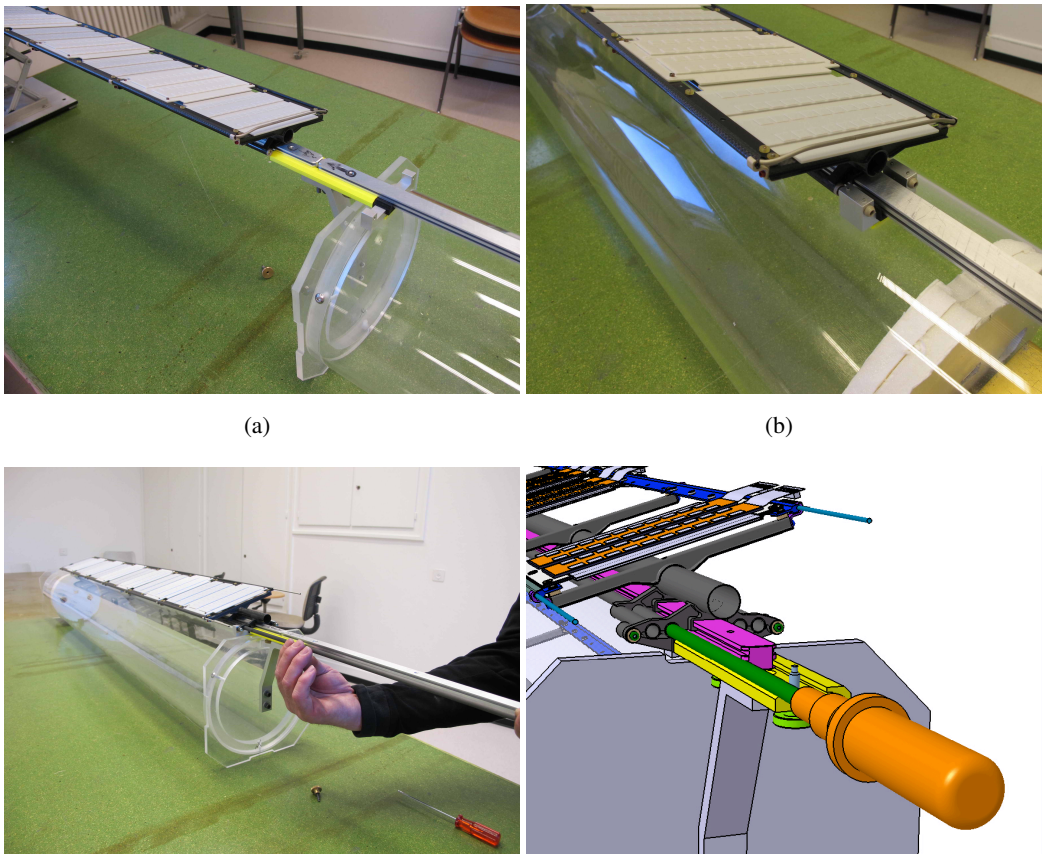

(a) (b)

(c) (d)

Figure 19. (a) The prototype SM on the temporary guiding rail, before being slid into position on the prototype GS cylinder. (b) The prototype SM after being slid into place but before locking. The $z = 0$ locking point is clearly visible. (c) Locking the SM in position with a long insertion tool guided by small CFRP tubes attached to the LS. (d) A 3-dimensional CAD view of the insertion tool guided by small cylindrical tubes on the LS.

2014 JINST 9 P04018

5 Finite Element Analysis (FEA) mechanical and thermo-mechanical studies

5.1 Overview

Using the ABAQUS software package [16], several FEA studies have been made on the mechanical and thermo-mechanical behaviour of the individual DSM modules, the LS and an assembled SM model including the LS and 12 DSM modules connected with their services. These studies have evolved in view of future DSM130 module developments and will further evolve to reflect the HL-LHC ATLAS tracker design.

5.2 The FEA model definition

The FEA model consists of a mixture of shell and solid elements, fabricated using both isotropic and orthotropic materials. Figure 20 shows the geometrical model used in the most recent mechanical and thermo-mechanical models. The applied loads and the boundary conditions depend on the detailed model comparisons. The DSM130 model (see section 3.1) includes: silicon wafers on each side of a TPG baseboard with glue layers, a hybrid definition based on the ABCN 130 nm CMOS front-end ASIC, and an aluminium nitride (AlN) facing with a thermal grease contact to the cooling plate. The same thermal grease is applied between the cooling pipes and the cooling plates. The thermal grease is modelled using a Young Modulus of 230 MPa to conservatively estimate the thermo-mechanical stresses in the LS following an integrated radiation dose expected for the HL-LHC ATLAS silicon strip tracker. The descriptions of links to the global support structure, the modules and cooling plate have been simplified to remove some non-structural details, but the model retains those elements relevant to mechanical and thermal behaviour. A solution that assumes no thermal grease between the DSM module and the cooling plate is also studied.

Table 3 lists the materials used for the FEA model, and the major material properties are shown in table 4. The FEA model allows the definition of a composite layup on a shell element from the material properties of a single ply.[12] This allows a study of the effect of different layup angles and thicknesses.

The boundary conditions of the model take into account the locking at 3 points along the SM when assembled onto a barrel. The $z \sim 1200$ mm contact at the end of the barrel is blocked. The other two attachment points allow the SM to slide in the longitudinal z-axis but the transverse and rotational degrees of freedom are blocked.

The attachment of modules to the cooling plates is implemented using dowel screws as shown in figure 3 (a). The design includes slots as shown in figure 21 and described in the text to allow for small CTE mismatches between the module and cooling plate, as well as to ease the module loading. They constrain all corners of the module in the y-axis (out of plane), but allow for bulk movements in the x-axis (lateral) and z-axis (longitudinal) degrees of freedom. FEA studies also exist for the case of a 4-point module constraint.

The cooling plate is an essential structural and a thermal element of the assembly and must therefore be optimised in both respects. Two options (see table 3) have been considered in the FEA studies below:

[12] M55J fibres are assumed for the FEA model.

2014 JINST 9 P04018

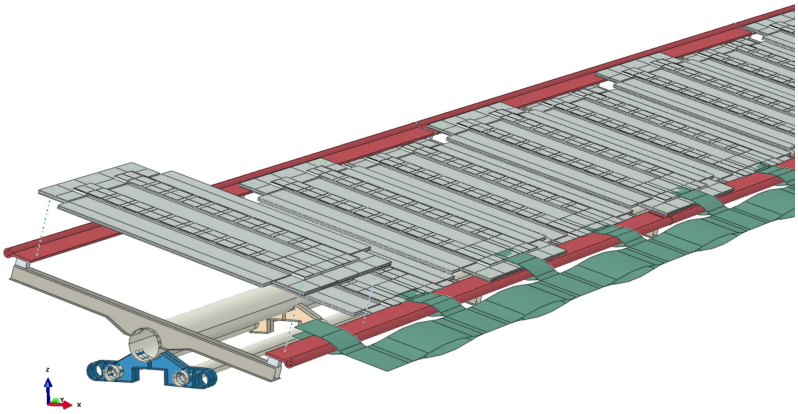

(a)

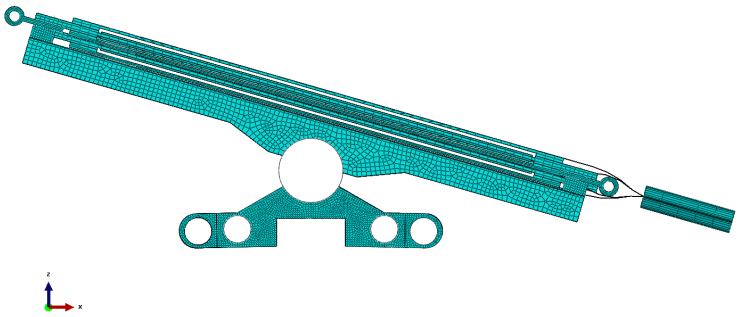

(b)

Figure 20. (a) The 3-dimensional model of the SM used as input for finite element analysis (FEA) studies. One module has been removed from the LS to show details of the model. (b) Cross-sectional view of the FEA model.

- The base-line material used in the existing design is the bi-directional Carbon-Carbon (CC2D) material that is machined to shape. It has an excellent in-plane thermal conductivity (360 W/mK) and a high Young's modulus (150 GPa). The existing design includes three separate cooling plates per side (six in total) as noted in section 3.5. Although the FEA model indicates good thermal performance (see section 5.4), the plates provide less rigidity for out-of-plane deformation under the effect of gravity after module loading, in particular at the cooling plate separations.

- An alternative design increasing the stiffness and simplifying the SM assembly foresees only one cooling plate per side. This could be CC2D, or a carefully designed layup of high stiffness and high thermal conductivity K13C fibres. The fibres in contact with the modules would be oriented to maximise the heat transfer between the cooling pipe and the modules. This design option is studied assuming a single CC2D plate to allow a comparison with the 3-segment baseline option. A detailed study of the required K13C layup and orientation is in progress.

2014 JINST 9 P04018

Table 3. Materials used in the FEA Model.

Part	**Material**	**Thickness (shell elements)**	**Comments**
Modules	Silicon wafers, kapton, conductive glue, AlN, TPG		Separate detailed model
Backbone wings	PEEK 1000	1 mm	Other thicknesses are also studied
Backbone tubes	M55J fibre composite layup	100 µm per ply	5 ply (0;20;-20;90;0 orientation) 3 ply also studied (0;90;0 orientation)
Transversal wings	M55J fibre fabric	100 µm per ply	3 ply (0;90;0 orientation) 2 ply layup (0;90) also studied
Interface blocks	PEEK 1000		
Cooling plates	Bi-directional CC2D		CC2D baseline CFRP layup also modelled using (0;90;0) fibre orientation
Service bus	Al and kapton	100 µm on wings 450 µm on wavy section	

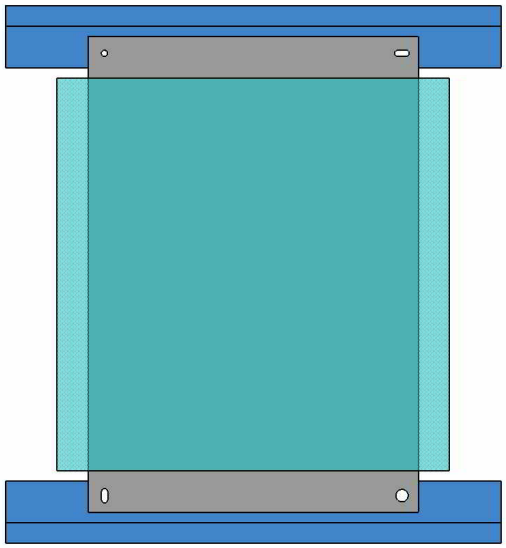

Figure 21. CAD view of the slotted attachment holes for mounting the DSM module base plate to the cooling plates. The fixed attachment is shown on the top left. The bottom right attachment allows movement in both the lateral and longitudinal directions.

Table 4. Major mechanical and thermo-mechanical properties used in the finite element (FEA) analysis model. In the case of non-isotropic properties, the subscripts apply to: i = 1 (in-plane longitudinal), i = 2 (in-plane lateral) and i = 3 (out of plane).

Material	**Part**	**Density** ($gm\ cm^{-3}$)	**Elastic Properties (GPa) Young Modulus E**	**Poisson Coefficient ν**	**Conductivity** ($Wm^{-1}\ ^oK^{-1}$)	**CTE** ($ppm\ ^oC^{-1}$)
Local Support						
CC2D or M55J layup	Cooling plates	1.9	$E = 150.0$	$\nu = 0.3$	$k_{1,2} = 360$ $k_3 = 0.035$	$\alpha_{1,2} = -0.45$ $\alpha_3 = 10$
M55J (1 ply)	Backbone + wings	1.67	$E_1 = 324.0$ $E_{2,3} = 5.0$	$\nu_{12} = 0.3$ $\nu_{13,23} = 0.1$	$k_1 = 300$ $k_{2,3} = 100$	$\alpha_1 = -0.5$ $\alpha_{2,3} = 30$
PEEK 1000	Spacers	1.32	$E = 6.0$	$\nu = 0.3$	$k = 1$	$\alpha = 10$
Titanium	Cooling tube	4.51	$E = 117.0$	$\nu = 0.3$	$k = 8$	$\alpha = 9$
Service bus (homogenised)		2.0	$E = 25.0$	$\nu = 0.3$	$k = 50$	$\alpha = 18$
Thermal grease	Cooling duct	1.3	$E = 0.23$	$\nu = 0.3$	$k = 1.5$	$\alpha = 5$
Module						
Silicon	$T = -40^oC$ $T = +40^oC$	3.2	$E = 340.0$	$\nu = 0.3$	$k = 0.21$ $k = 0.13$	$\alpha = 3.0$
AlN		2.3	$E = 112.0$	$\nu = 0.3$	$k = 180.0$	$\alpha = 4.5$
Kapton		1.3	$E = 13.0$	$\nu = 0.34$	$k = 40.0$	$\alpha = 18.0$
Conductive glue		1.3	$E = 7.0$	$\nu = 0.3$	$k = 2.8$	$\alpha = 25.0$
TPG	$T = -40^oC$	1.3	$E = 83.0$	$\nu = 0.34$	$k_{1,2} = 2010$ $k_3 = 6$	$\alpha_{1,2} = -1.2$ $\alpha_3 = 25.0$
TPG	$T = +40^oC$	1.3	$E = 83.0$	$\nu = 0.34$	$k_{1,2} = 1530$ $k_3 = 6$	$\alpha_{1,2} = -1.2$ $\alpha_3 = 25.0$

The thermal transport is sensitive to the contact between the cooling plate and the DSM modules. The FEA model assumes a 50 μm layer of heat-transfer grease with conductivity k=1 W/mK uniformly spread across the surface. Comparisons have been made with a 2-point direct contact on each side of the module, without the use of thermal grease.

As discussed in section 3.6, the service bus design and assembly is also a key issue that has not been optimised. The base-line FEA model foresees a relatively rigid service bus supported by rigid wings as shown in figure 13. These wings ensure electrical contact between the service bus and modules as well as mechanical support for the bus. However, the bus imposes significant stress on the modules and transfers any thermo-mechanical instabilities to the modules. The FEA analyses below indicate the influence of the service bus on the stability of the module positioning.

The following sections present results obtained by FEA analyses under various conditions, in an attempt to establish viability of the original design, as well as the importance of the design suggestions above for the 2 aspects not yet fully optimised: the cooling plate and the service bus. The model used varies slightly between analyses, but the main characteristics remain unchanged.

2014 JINST 9 P04018

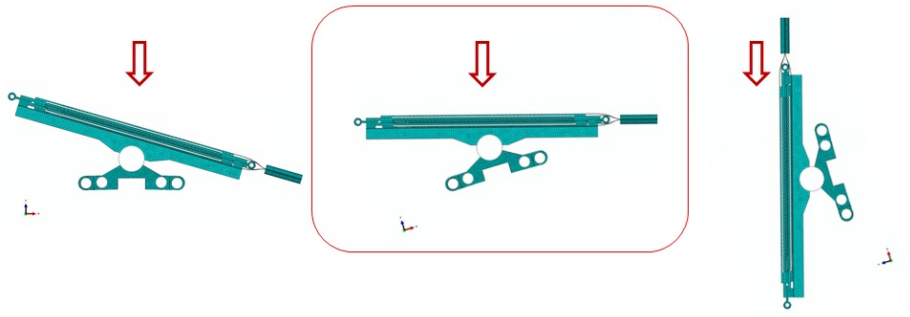

Figure 22. Orientation of the SM (shown in blue) with respect to gravity. The highlighted orientation is a worst-case scenario to describe the SM sagging under full load.

5.3 Finite Element Analysis models of the mechanical stability

The mechanical FEA study has been made using 3 different load cases, as shown in figure 22. The gravity sag perpendicular to the module plane is by far the worst-case scenario and is described below. A previous dynamic analysis, using the same local support but with a different DSM module model (ABCN250), indicated a first Eigen frequency of ~ 55 Hz. This is however dependent on the attachment.

Table 5 indicates the expected maximum SM deformation at a temperature of 20 ^{o}C from gravitational sag, in the case of a LS using a 5-ply CFRP layup for the support central tube of the LS (the mechanical prototyping used a 3 ply CFRP layup for this component). Several comparisons are considered:

- The effect on using 3 separated CC2D cooling plates (baseline) as compared to a single C-C cooling plate (comparison of configurations 2 and 4);
- The influence on the deformation of the service bus using the baseline model described above (comparison of configurations 2 and 3, or 4 and 5);
- The influence on the deformation of using fixed module attachments, as compared to sliding module attachments (comparison of configurations 1 and 2).

Given the 3-point fixation configuration of the SM to the general structure, the maximum displacement of the baseline configuration 2 is 56 µm. In the case of configuration 2 using a 3-ply central support tube, the maximum displacement increases to 70 µm. The improvement of the maximum displacement on the choice of module fixation to the cooling plates is small: from 56 µm to 54 µm. However, the contribution of the cable bus to the maximum displacement ($\sim$ 10 µm) is large and requires further optimisation. Figure 23 shows the mapping of the total displacement due to the gravitational load perpendicular to the module plane, for the end 4 modules from configuration 2 listed in table 5. As expected the maximum displacement is mid-way between the fixation points.

Because of computing time and space limitations, the effect on the expected stress due to the mesh size has been studied, but no issue related to the stress with respect to the gravity load has been identified. The number of elements when the full model is used (including the service bus) is 965078 and the number of nodes for the full model is 1198263.

2014 JINST 9 P04018

Table 5. Maximum expected SM displacement in each of the in-plane lateral (x-axis) and longitudinal (z-axis) directions and the out-of-plane (y-axis) direction due to gravitational sag, including the effect of the service buses but excluding the deformation of the service buses themselves. All results are in units of μm. The numbers in brackets indicate the expected maximum module displacement.

Configuration	**Cooling Plate**	**Module Attachment**	**Service Bus**	Deflection (μm)			
				$\lvert\Delta\rvert$	$\lvert\Delta_x\rvert$	$\lvert\Delta_y\rvert$	$\lvert\Delta_z\rvert$
1	CC2D	Fixed	Yes	54(54)	13(13)	53(52)	1.8(0.8)
2	CC2D	Sliding	Yes	56(55)	13(13)	54(54)	1.8(0.8)
3	CC2D	Sliding	No Service Bus	49(49)	14(14)	47(47)	1.6(0.7)
4	CFRP layup (C-C)	Sliding	Yes	54(53)	13(14)	52(51)	1.7(0.9)
5	CFRP layup (C-C)	Sliding	No Service Bus	45(45)	14(13)	43(43)	1.6(0.8)

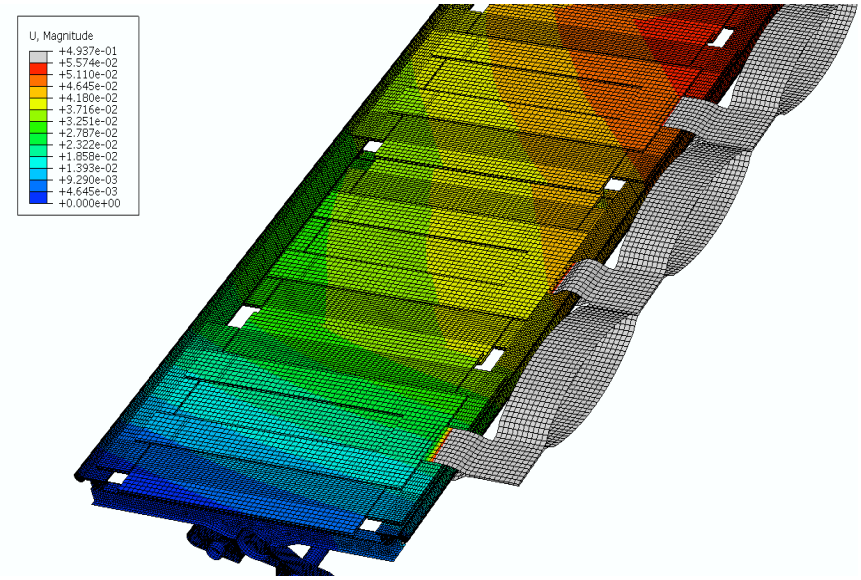

Figure 23. Mapping of the total displacement due to the gravitational load perpendicular to the module plane, in the case of configuration 2 as listed in the text. The mapping includes the effect of the service buses, but the service bus deformation is not shown.

To fully validate the SM approach, load test measurements have been made on SM prototype (see the schematic of figure 24 (a)). In this case the loaded SM included:

- the 12 dummy modules fabricated from polyurethane for LS assembly studies;
- the 6 cooling plates fabricated from aluminium and fitted with titanium cooling pipes as in configuration 2;
- the SM support frame made from CFRP and close to the expected design.

Measurements of the resulting deflections for different loads were made using dial comparators (4 independent simultaneous measurements for each load case). The load was applied uniformly

2014 JINST 9 P04018

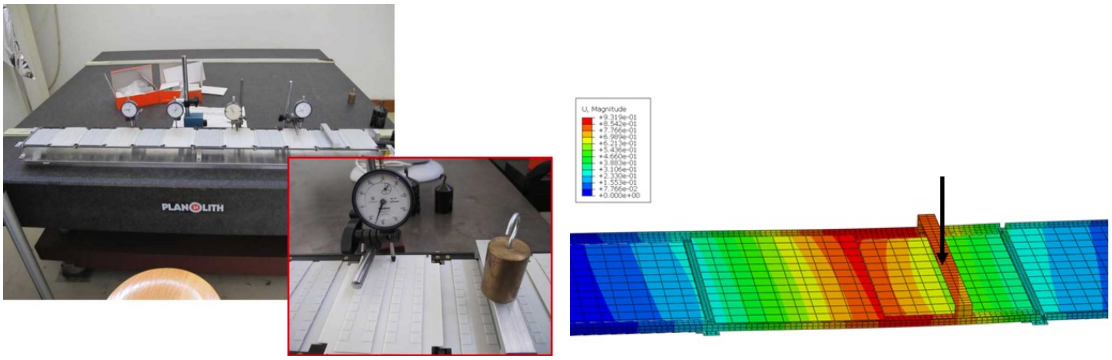

(a) (b)

Figure 24. (a) Photograph of the test measurement, and (b) the corresponding expected mechanical distortion from a finite element (FEA) analysis model following a 1000 gm load.

across the module width at 5 different locations along the SM, using an aluminium cross-bar attached to a calibrated brass cylinder. The actual materials of the prototype were carefully measured, and were input into the FEA model (slightly simplified) for comparison with the measurements.

Figure 24 (b) shows the result of one FEA simulation, taking into account the different materials used, for an applied load of 1000 gm. The expected FEA deflection of $0.5-0.6$ mm is within 20% of the maximum measured deflection of 0.65 mm. A fully loaded thermo-mechanical prototype, including silicon-based thermo-mechanical modules of the final DSM design, will be required to allow an accurate measurement of the stresses, deflections and temperature gradients along the SM. However, on the basis of experience gained so far, the FEA model is expected to be an realistic representation of the SM design.

5.4 Finite Element Analysis models of the thermo-mechanical stability

During the operating lifetime of a fully loaded SM, all components will be subjected to large temperature variations, due to the heat generated by the on-detector electronics, and to the increased sensor leakage current following irradiation that necessitates operation at sensor temperatures of $\leq -20\ ^{o}$C.

For the 5 configurations already noted in table 5, a FEA steady-state thermo-mechanical analysis has been made for the fully loaded SM (no transient analyses have yet been made). As previously described, the DSM and SM mechanics have been designed to minimise thermo-mechanical displacements by kinematically separating materials having a large CTE-mismatch. The materials having the highest CTE in the SM design are the service bus and the PEEK support blocks. The evaporative cooling system is based on CO_2 with a coolant temperature of $-35\ ^{o}$C, and a titanium cooling tube of inner diameter 2 mm, with HTCP grease surrounding the cooling pipes with an assumed elastic modulus of 230 MPa.

The FEA model assumes an initial steady state temperature for all components of $T = 20\ ^{o}$C. The final steady state conditions assume the mechanical boundary conditions previously described and:

- A convection state on the inside of the cooling tube at the cooling plate of $T = -35\ ^{o}$C and a heat transfer coefficient to the cooling plate of $h = 8000\ Wm^{-2}K^{-1}$;

2014 JINST 9 P04018

Table 6. Maximum expected SM displacement in each of the in-plane lateral (x-axis) and longitudinal (z-axis) directions and the out-of-plane (y-axis) direction due to the combined effects of thermal load and gravitational sag. All results are in units of μm. The numbers in brackets indicate the expected maximum module displacement. The effect of the service bus is included in the model, but the deformations of the service bus are not shown.

Configuration	**Cooling Plate**	**Module Attachment**	**Service Bus**	Deflection (μm)			
				$\lvert\Delta\rvert$	$\lvert\Delta_x\rvert$	$\lvert\Delta_y\rvert$	$\lvert\Delta_z\rvert$
1	CC2D	Fixed	Yes	70(65)	19(18)	67(62)	21(21)
2	CC2D	Sliding	Yes	58(58)	15(15)	55(55)	14(14)
3	CC2D	Sliding	No	57(57)	16(14)	56(56)	14(14)
4	CFRP layup (C-C)	Sliding	Yes	69(69)	24(19)	65(63)	25(25)
5	CFRP layup (C-C)	Sliding	No	61(61)	21(18)	57(57)	25(25)

- Heat fluxes (power losses) on the module electronics of 0.0055 $\mathrm{Wmm^{-3}}$ for each DC-DC unit, 0.0033 $\mathrm{Wmm^{-3}}$ for each ABCN 130 front-end ASIC and 0.0029 $\mathrm{Wmm^{-3}}$ for other electronics components;

- A convection condition due to dry air on the module interface of $\mathrm{T} = 0\ ^{\mathrm{o}}\mathrm{C}$ with a heat transfer coefficient $\mathrm{h} = 5\ \mathrm{Wm^{-2}K^{-1}}$ (the mean of horizontal and vertical convection coefficients); and

- The temperature at each interface with the global support is fixed at $\mathrm{T} = 0\ ^{\mathrm{o}}\mathrm{C}$.

The maximum steady-state displacements expected for each configuration are shown in table 6. A mapping of the out-of-plane displacement due to the thermo-mechanical load is shown in figure 25 for the case of configuration 2 in table 6. In this case, there is additional lateral displacement due to the small but non-zero CTE of the DSM module components. A comparison of the deformations for configurations 1 and 2 illustrates the importance of kinematic module attachment to the cooling plates. A comparison between configurations 2 and 4 indicates the need to retain a low CTE for the cooling plate if a single unit is used.

The deformations result mainly from the LS structure, and those internal to the module are small. The maximum in-plane deformation for a temperature variation $\Delta\mathrm{T} = 40\ ^{\mathrm{o}}\mathrm{C}$ is less that 14.5 μm (< 1.5 μm deformation for a 5 $^{\mathrm{o}}\mathrm{C}$ temperature variation) and the out-of-plane deformation is less that 1.5 μm.

The effect of the external convection temperature has been modelled using temperatures of ($-10\ ^{\mathrm{o}}\mathrm{C}$, $0\ ^{\mathrm{o}}\mathrm{C}$, and $+10\ ^{\mathrm{o}}\mathrm{C}$ and a convection heat transfer coefficient $\sim 5\ \mathrm{Wm^{-2}\ ^{o}K^{-1}}$), to estimate the influence on the temperature of the silicon wafer . The contact temperature at the LS locking point and the global structure is fixed to that of the convection temperature. The maximum deflections in the 3 cases (configuration 2), as well as the sensor temperature range, are shown in table 7. The temperature mapping on the overall structure is shown in steady-state condition assuming a coolant temperature of $\mathrm{T} = -35\ ^{\mathrm{o}}\mathrm{C}$ and an environmental temperature of $\mathrm{T} = 0\ ^{\mathrm{o}}\mathrm{C}$, in figure 26 a). Figure 26 b) shows a temperature map on a DSM sensor evaluated under the same conditions. The mean sensor temperature is however sensitive to the assumed thermal contact between the cooling plate and the DSM module, in this case assuming full thermal contact. In the

2014 JINST 9 P04018

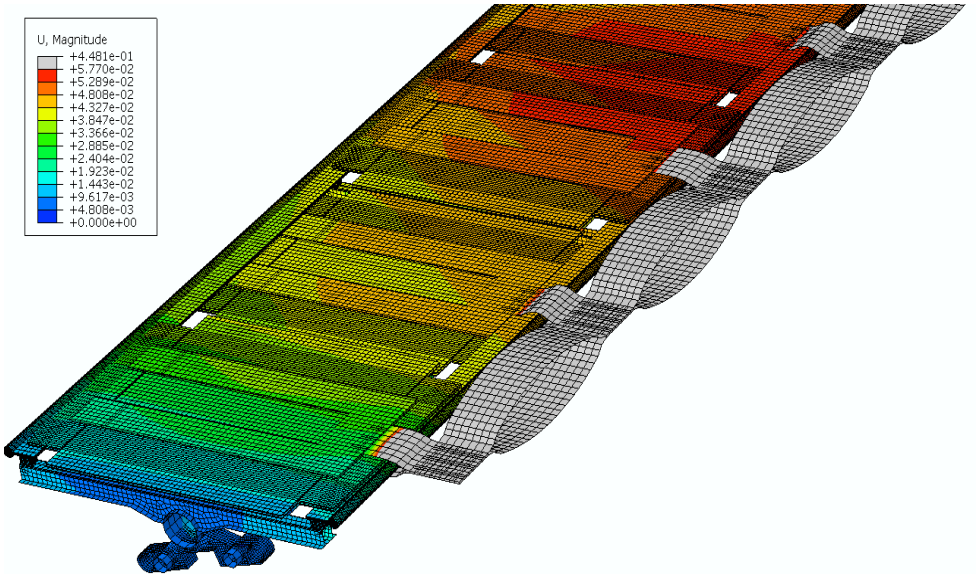

Figure 25. Mapping of the total displacement due to the combined effects of gravitational sag and thermal load, in the case of configuration 2 as described in the text. The effect of the service bus is included in the model, but the deformations of the service bus are not shown.

Table 7. Sensitivity of the maximum expected SM displacement (configuration 4) with respect to an unpowered SM at T = 20 °C, in each of the in-plane lateral (x-axis) and longitudinal (z-axis) directions and the out-of-plane (y-axis) direction, to changes in the environmental temperature. All results are in units of µm. Deformations of the service bus are not included. The maximum sensor temperature is also shown. The assumed coolant temperature is T = −35 °C.

Environment Temperature (°C)	**Sensor Temperature** (°C)	Deflection (µm) $\lvert\Delta\rvert$	$\lvert\Delta_x\rvert$	$\lvert\Delta_y\rvert$	$\lvert\Delta_z\rvert$
-10	-31.6 – -32.0	71	25	66	67
0	-31.3 – -31.8	69	24	65	25
+10	-31.1 – -31.7	64	22	63	24

pessimistic case of a direct contact to the cooling plate only at the attachment holes, a sensor temperature between −25.3 °C and −26.7 °C is calculated. If the hybrid is glued directly to the sensor, the average sensor temperature is also increased by $\sim$ 4 °C.

As a starting point in the FEA calculations described, the service bus characteristics are assumed to be those of the IBL service bus [14]. Further optimisations of its shape are required to limit the longitudinal stress and any consequent deflection of the modules.

Another region of longitudinal thermo-mechanical stress is the thermal grease contact region between the cooling plate and the cooling pipe to estimate the stress in this region. Assuming a Young's modulus for the thermal grease of 230 MPa following irradiation, a maximum of 2 MPa has been calculated on the grease joint at the very end of the cooling plate. In the extreme (unrealistic) case of a Young's modulus 3000 MPa, the displacement is changed by only a few µm.

2014 JINST 9 P04018

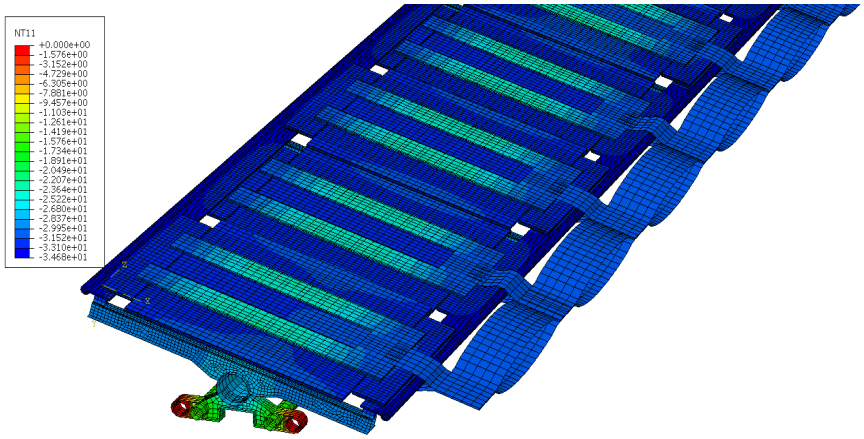

(a)

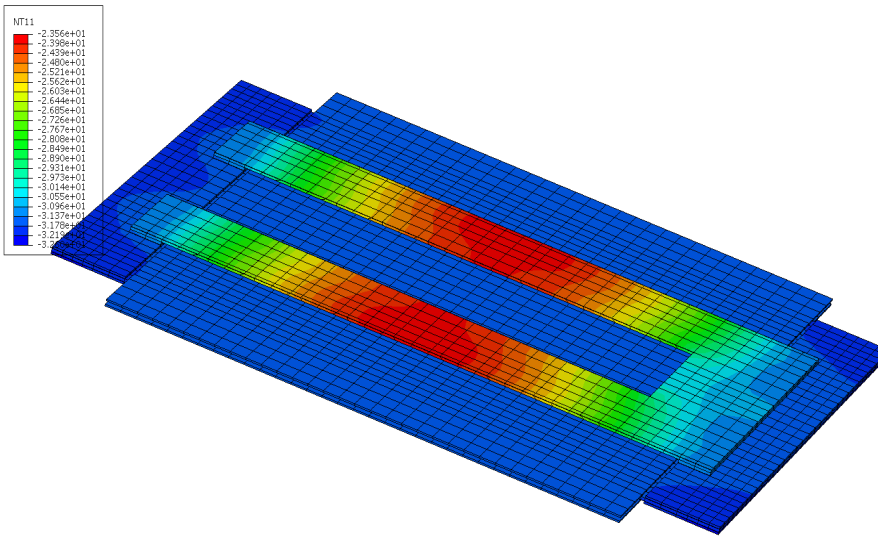

(b)

Figure 26. a) Temperature mapping of the SM with its LS, and b) the DSM sensor itself, assuming a CO_2 coolant at -35^oC and an environmental (convection) temperature of 0 ^oC.

6 Expected material budget of the super module

The expected material budget is shown in table 8. Excepting the service bus, this is a conservative estimate based on well-characterised materials of known thermo-mechanical properties. It is expected that the material budget can be further optimised. The module material in particular includes silicon sensors of 320 µm thickness (as opposed to 285 µm for the existing detector).

The service bus layout, one option of which is shown in figure 14, will be based on the current IBL stave flex, as discussed in section 3.6. Averaged over the SM active area, the service material budget is expected to be 0.11% X_0 , as shown in table 9. The material estimate includes the stiffener used at the pigtail connector for individual modules.

2014 JINST 9 P04018

Table 8. Expected material budget (% X_0) for separate major components of the SM and LS, including the double-sided modules. The quoted budget does not include the SMC electronics card and associated mechanics, but it does include all mechanical attachments to the support barrels.

Item	**Radiation Length** % X_0	
Module with CC bridge (12 mm width)	-	1.59
Module without CC bridge	1.49	-
Local Support	0.18	0.18
Cooling plates	0.17	0.17
Cylinder interface (brackets, inserts)	0.08	0.08
Titanium cooling pipe (ID 2 mm)	0.04	0.04
Service Bus	0.11	0.11
Total	**2.07**	**2.17**

Table 9. Breakdown of the expected service bus material budget (% X_0).

Item	**Radiation Length** % X_0
Al layers - GND and bias (100 µm)	0.0174
Kapton + glue (240 µm)	0.0136
Cu layers ($\sim$ 10 µm)	0.0155
Stiffeners (22 x 13 x 0.3 mm^3)	0.0029
Connectors	0.005
Total (1 side)	0.0544
Total (2 sides)	**0.1088**

7 Summary

This report summarises mechanical and thermo-mechanical results in the first phase of an development program to establish the suitability of a double-sided silicon micro-strip module (DSM) development for the Inner Tracker (ITK) of the ATLAS experiment at the HL-LHC. The development foresees the construction of DSM modules attached to a light but stable carbon-fibre based local support (LS) that provides a precise mechanical support for the DSM modules, and together with loaded DSM modules and their associated services is attached to carbon fibre cylinders in the central (barrel) region of the ITK.

The development has used the result of a complementary electronics project (the ABCN 250 nm CMOS front-end ASIC) [10] to construct double-sided micro-strip silicon modules (DSM250), that have been operated successfully in a so-called 8-module electrical prototype [5, 6, 9]. The DSM250 modules have been demonstrated to fulfil the electrical requirements for the HL-LHC tracker, but detailed design work is still required for the optimised service design. The next step of the electrical development will be the construction of DSM130 modules, using the ABCN 130 nm CMOS ASIC now in fabrication, and the full characterisation of a multi-module electrical SM using an optimised service layout and readout electronics.

The other aspect of the project has been the demonstration of a light and stable support for the DSM modules, as described in this report. This has involved the design, construction and characterisation of DSM modules mounted on a local support (LS) that when loaded with DSM

2014 JINST 9 P04018

modules and services (the Super Module, or SM) can be can inserted into a global support structure (GS). The prototypes, together with design studies and finite element analyses (FEA) indicate that mechanical specifications of the ITK at the level of those for the existing SCT can be achieved. The next step of the project is to load DSM130 modules onto an evolved design of the LS and to repeat the electrical and mechanical studies required to validate a viable design for the ATLAS ITK. Excepting detailed service bus design optimisations, the viability of the DSM module and LS concept has been demonstrated.

As a result, FEA studies have been made to understand and optimise the expected mechanical and thermo-mechanical behaviour of DSM130 modules loaded onto an evolved LS and SM design, based on its behaviour under set conditions using a worst-case gravitational sag configuration (in practice, the SM units will be assembled around the perimeter of a barrel structure and the effect of sag will be reduced). A $\sim$ 55 µm maximum out-of-plane displacement is expected, using a 3-point kinematic attachment. The in-plane movements are minimal. However the FEA model assumes a 5-ply CFRP layup for the LS backbone tube; for a 300 µm thick backbone tube layup as in the original design, the maximum out-of-plane displacement is 70 µm.

Gravity sag is also included in the thermo-mechanical FEA model; in this case the mechanical variations resulting from the operating temperature are added. The out-of-plane displacement is almost unchanged but in-plane displacements are increased. These displacements result from the CTE behaviour of individual modules, and the coupled stresses induced by the cooling pipe and service bus, that must be minimised.

Two features remain under investigation; the cooling plate design and the service bus:

- A single CFRP cooling plate per side, manufactured from a composite carbon fibre layup, would have several advantages if it could be fabricated with an adequate thermal conductivity, and a CTE value very close to zero. As well as increasing the rigidity, it might allow the cooling tube to be embedded in the layup, allowing a reduced cooling pipe thickness and improved thermal coupling to the plate. This option requires both mechanical and thermo-mechanical validation.

- The basic concept of the service bus exists, and the electrical SM prototype has demonstrated an initial prototype service bus. However, an optimised design with good mechanical stability but minimal material, as well as good electrical reliability, remains an important goal of the future DSM130 module program.

The detailed FEA model is now available to perform further studies of both steady-state and dynamical thermo-mechanical behaviour (for example transient analyses of the thermo-mechanical stability following changes of the coolant temperature or changes to the electronic power load).

Acknowledgments

This research was partly supported by by the JSPS Grant-in-Aid for Scientific Research (A) [No. 20244038] and (C) [No. 20540291], MEXT Grant-in-Aid for Scientific Research in Priority Area [No. 20025007] and on Innovative Areas [No. 23104002], Japan. We also acknowledge the financial support of the State Secretariat for Education, Research and Innovation, the Swiss National Science Foundation and the Canton of Geneva, Switzerland.

2014 JINST 9 P04018

References

[1] ATLAS collaboration, G. Aad et al., *The ATLAS Experiment at the CERN Large Hadron Collider*, 2008 *JINST* **3** S08003.

[2] ATLAS collaboration, *Letter of Intent for the Phase-II Upgrade of the ATLAS Experiment*, CERN-LHCC-2012-022 (2012).

[3] ATLAS collaboration, *Final Report: ATLAS Phase-2 Tracker Upgrade Layout Task Force*, ATL-UPGRADE-PUB-2012-004 (2012).

[4] ATLAS collaboration, *Silicon strip staves and petals for the ATLAS Upgrade tracker of the HL-LHC*, *Nucl. Instrum. Meth.* **A 699** (2013) 93.

[5] S. Gonzalez-Sevilla, G. Barbier, F. Anghinolfi, F. Cadoux, A. Clark et al., *A silicon strip module for the ATLAS inner detector upgrade in the super LHC collider*, *Nucl. Instrum. Meth.* **A 636** (2011) S97.

[6] S. Gonzalez-Sevilla, A.A. Affolder, P.P. Allport, F. Anghinolfi, G. Barbier et al., *A double-sided silicon micro-strip Super-Module for the ATLAS Inner Detector upgrade in the High-Luminosity LHC*, 2014 *JINST* **9** P02003.

[7] A. Abdesselam, P.P. Allport, C. Anastopoulos, B. Anderson, L. Andricek et al., *The integration and engineering of the ATLAS SemiConductor Tracker barrel*, 2008 *JINST* **3** P10006.

[8] ATLAS collaboration, *Study of alignment-related systematic effects on the ATLAS Inner Detector tracking*, ATLAS-CONF-2012-141 (2012).

[9] ATLAS collaboration, *Electrical results of double-sided silicon strip modules for the ATLAS Upgrade Strip Tracker*, ATL-UPGRADE-PUB-2012-002 (2012).

[10] F. Anghinolfi et al., *Performance of the ABCN-25 readout chip for the ATLAS Inner Detector Upgrade*, Proceedings of the Topical Workshop on Electronics for Particle Physics (TWEEP-09), CERN-2009-006 (2009).

[11] ATLAS collaboration, *Design and assembly of double-sided silicon strip module prototypes for the ATLAS upgrade strip tracker*, ATL-UPGRADE-PUB-2011-002 (2011).

[12] P. Miyagawa and I. Dawson, *Radiation background studies for the Phase II inner tracker Upgrade*, ATL-UPGRADE-PUB-2013-012 (2013).

[13] ATLAS collaboration, *Thermal Grease Evaluation for ATLAS Upgrade Micro-Strip Detector.*, ATL-UPGRADE-PUB-2010-002 (2010).

[14] ATLAS Collaboration, *ATLAS Insertable B-Layer Technical Design Report*, CERN-LHCC-2010-0013, CERN, Geneva, September 2010.

[15] ATLAS collaboration, *System Electronics for the ATLAS Upgraded Strip Detector*, ATL-UPGRADE-PUB-2013-011 (2013).

[16] ABAQUS Software from Simulia Dassault Systems, *Tool for multi physics FEA simulation*, http://www.simulia.com/products/multiphysics.html.

2014 JINST 9 P04018